CORROSION DETECTION AND PREDICTION STUDIES

A Thesis

by

SALLY SAMIR FARID NICOLA

Submitted to the Office of Graduate Studies of
Texas A&M University
in partial fulfillment of the requirements for the degree of

MASTER OF SCIENCE

August 2012

Major Subject: Safety Engineering

Corrosion Detection and Prediction Studies

Copyright 2012 Sally Samir Farid Nicola

CORROSION DETECTION AND PREDICTION STUDIES

A Thesis

by

SALLY SAMIR FARID NICOLA

Submitted to the Office of Graduate Studies of
Texas A&M University
in partial fulfillment of the requirements for the degree of

MASTER OF SCIENCE

Approved by:

Chair of Committee,	M. Sam Mannan
Committee Members,	James C. Holste
	Eric L. Petersen
Head of Department,	Charles Glover

August 2012

Major Subject: Safety Engineering

ABSTRACT

Corrosion Detection and Prediction Studies. (August 2012)

Sally Samir Farid Nicola, B.S., Texas A&M University at Qatar

Chair of Advisory Committee: Dr. M. Sam Mannan

Corrosion is the most important mechanical integrity issues the petrochemical industry has to deal with. While significant research has been dedicated to studying corrosion, it is still the leading cause of pipeline failure in the oil and gas industry. Not only is it the main contributor to maintenance costs, but also it accounts for about 15-20% of releases from the petrochemical industry and 80% of pipeline leaks. Enormous costs are directed towards fixing corrosion in facilities across the globe every year. Corrosion has caused some of the worst incidents in the history of the industry and is still causing more incidents every year. This shows that the problem is still not clearly understood, and that the methods that are being used to control it are not sufficient.

A number of methods to detect corrosion exist; however, each one of them has shortcomings that make them inapplicable in some conditions, or generally, not accurate enough. This work focuses on studying a new method to detect corrosion under insulation. This method needs to overcome at least some of the shortcomings shown by the commercial methods currently used. The main method considered in this project is X-ray computed tomography. The results from this work show that X-ray computed tomography is a promising technique for corrosion under insulation

detection. Not only does it detect corrosion with high resolution, but it also does not require the insulation to be removed. It also detects both internal and external corrosion simultaneously.

The second part of this research is focused on studying the behavior of erosion/corrosion through CFD. This would allow for determining the erosion/corrosion rate and when it would take place before it starts happening. Here, the operating conditions that led to erosion/corrosion (from the literature) are used on FLUENT® to predict the flow hydrodynamic factors. The relationship between these factors and the rate of erosion/corrosion is studied. The results from this work show that along with the turbulence and wall shear stress, the dynamic pressure imposed by the flow on the walls also has a great effect on the erosion/corrosion rate.

DEDICATION

To my father, my mother, my brother, and my sisters

ACKNOWLEDGEMENTS

I would like to thank my committee chair, Dr. Mannan for the guidance, encouragement, advice and inspiration, and my committee members, Dr. Holste, and Dr. Petersen, as well as my mentor, Dr. Carreto, for their guidance and support throughout the course of this research.

I would also like to thank my friends and colleagues and the department faculty and staff for all their support and for making my experience truly memorable.

Last but certainly not least, I would like to thank my father, Samir Nicola, and my mother, Magda Nicola for their unconditional love, encouragement, patience, and advice, and for always believing in me and inspiring me. I would also like to thank my siblings Dina, Rana and Mina for their continuous love, support and companionship.

NOMENCLATURE

β	Coefficient of thermal expansion
C_μ, C_1, $C_{1\varepsilon}$, C_2, $C_{2\varepsilon}$	Constants for the k-epsilon model
ε	Turbulence dissipation rate
g_i	Gravity
k	Turbulent kinetic energy
μ	Dynamic viscosity
p	Node
ρ	Density
P_{rt}	Prandtl number for energy
y_p	Distance from point p to the wall
u	Axial velocity

TABLE OF CONTENTS

LIST OF FIGURES

LIST OF TABLES

1. INTRODUCTION

1.1 Introduction

Corrosion has become one of the most important mechanical integrity issues the petrochemical industry has to deal with. While significant research has been dedicated to studying the mechanisms of the different kinds of corrosion, methods to avoid it, and methods to monitor, it is still the leading cause of pipeline failure in the oil and gas industry. It comes in different forms and each form can happen due to different reasons, which make it much more complicated than simply a chemical reaction. A study that was carried out in 2002 revealed that direct costs of corrosion make up to 3.1% of the Gross Domestic Product (GDP) of the US (Koch and Thompson, 2002). Not only is it the main contributor to maintenance costs, but also it accounts for about 15-20% of releases from the petrochemical industry and 80% of pipeline leaks. Moreover, enormous costs are directed towards fixing corrosion in facilities across the globe every year. An average of about 8000 corrosion leaks are repaired every year on natural gas pipelines, and about 1600 spills per year are repaired and cleaned up for liquid products (Beavers and Thompson, 2006). Another study that was carried out by PHMSA, reported that in 2004, 258 natural gas incidents took place due to corrosion in pipelines (Keeping Pipelines Safe from Internal Corrosion, 2011).

This thesis follows the style of *Journal of Loss Prevention in the Process Industries.*

Some of the recent incidents that were caused by corrosion are discussed in the next section.

1.2 Corrosion Incidents

Corrosion has caused some of the worst incidents in the history of the industry, such as the Carlsbad pipeline explosion of 2000, and it is still causing more incidents every year. These incidents lead to significant economic losses and also jeopardize the safety of the personnel and the process equipment. In this section, some of the incidents that were caused by corrosion will be discussed.

According to the European Major Accident Reporting System (MARS), corrosion was responsible for 21.5% of all the incidents that were reported to the database. Studies showed that corrosion incidents in refineries the EU caused more than $2.2 billion in property damage. The following figure shows the corrosion case distribution until 2009 (Wood, 2010).

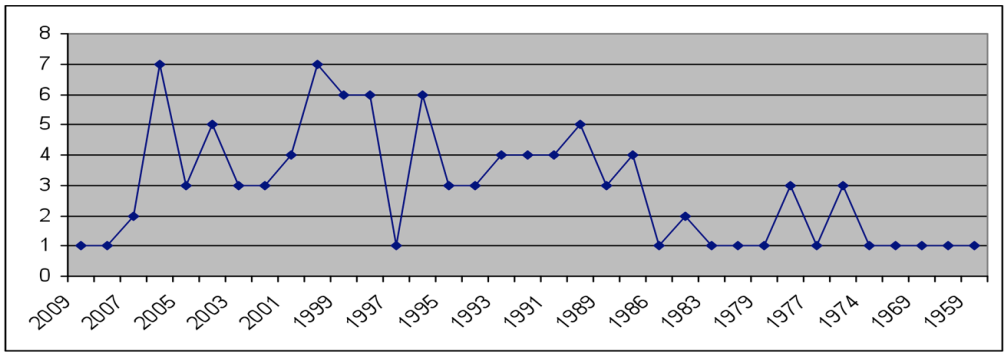

Figure 1: Corrosion Cases by Year (Wood, 2010)

Figure 1 shows a general increasing trend for the number of corrosion-related incidents happening with time. Some of the major incidents that have occurred after 2005 are summarized in the following few paragraphs.

On July 22, 2006, a rupture in a 24-inch gas line led to the release of about 43,000 MSCF of natural gas, near Clay City in Clark County, Kentucky. The release led to a fire that lasted about an hour. While no fatalities or injuries occurred, three homes had to be evacuated and some nearby properties experienced some minor damages as a result of the release and the fire. Investigations then showed that external pitting corrosion was covering 2-3 ft near the rupture (Department of Transportation Pipeline and Hazardous Materials Safety Administration Office of Pipeline Safety, 2006).

During 2008 several other incidents related to corrosion took place. One of them is the Cooper County, Missouri natural gas pipeline rupture. This incident took place on August 29, 2008, a day after the Shairtown, Texas incident. Here a 24-inch gas

transmission pipeline failed releasing about 13.5 million CF of natural gas. While this incident led to no injuries or fatalities, it led to property damage that cost about $ 25,000 with much higher associated damages cost. Investigations later on showed that external corrosion was taking place at the pipe at the rupture area and had worn out about 75% of the walls. The figure opposite shows external corrosion at the possible origin of the rupture (CC Technologies, 2008). Also in 2008 another incident related to corrosion took place in Appomattox, Virginia. On September 14, a 30-inch natural gas pipeline ruptured causing a large fireball that led to a burn zone of about 1125 ft in diameter. 23 families had to evacuate and two roads had to be closed. The fire injured 5 individuals, destroyed 2 houses and damaged hundreds (Department of Transportation Pipeline and Hazardous Materials Safety Administration, 2008).

PHMSA fined the company operating the line with $952,500 for failing to address the regulatory requirements for monitoring and preventing external corrosion (Sidener, 2009). In 2010, another incident caused by corrosion took place on April 5 in Green River, Wyoming. Pressure in a corroded pipeline caused the pipe to rupture and spill about 84,000 gallons of crude oil. The oil leaked into an irrigation ditch and contaminated the soil (Federation, 2010).

1.3 Objective

The industry has been struggling with corrosion since as early as the 1800's. Even though numerous studies have been conducted to understand and quantify the corrosion problem, incidents are still happening that indicate that the problem has not yet been resolved. The main objective of this work is to study methods of detection for some of the common types of corrosion, as well as to implement CFD modeling in order to be able to estimate the amount of corrosion happening, in order to help schedule maintenance. These methods must overcome the shortcomings of the commercial methods currently used by the industry, which will be discussed in a later chapter.

2. TYPES OF CORROSION

2.1 Introduction

Corrosion is the chemical degradation of a material by the environment surrounding it. It can come in different forms and grow at different rates. To begin understanding the extent of the corrosion problem, it is important to first know the mechanisms by which the damage starts taking place. The problem is that many forms of corrosion exist and each is caused by different reasons and undergoes different mechanisms. Moreover, each form of corrosion has its own special mechanism, which can be quite complex in some cases. This is especially problematic when two or more types of corrosion take place simultaneously. Some of the common types of corrosion and their mechanisms will be discussed in the following few sections.

2.2 Generalized Corrosion

Generalized corrosion (also known as “uniform corrosion”) is a form of corrosion that affects the entire surface of the metal, whereas other forms affect a specific spot or portion. It is a very slow reaction that is fairly evenly distributed over the entire metal surface exposed to any circulating water. The fact that it affects a fairly large area of the metal makes it much easier to detect, and hence much less severe than localized corrosion. The problem with generalized corrosion is that it results

in a large volume of oxides that tend to attach themselves to the heat transfer surfaces and affect the efficiency of the system (Hansen, et al., 2009) (Piper, 1999).

2.3 Pitting Corrosion

Pitting corrosion is the form of corrosion that occurs in isolated parts of the metal. It is concentrated to very small areas and affects the useful life of the equipment itself. The fact that it is localized makes it harder to detect and therefore can be undetected for long periods, making the equipment more prone to severe damage. This makes pitting corrosion the most severe form of corrosion (Piper, 1999).

2.4 Galvanic Corrosion

Galvanic corrosion (also known as dissimilar metal corrosion) is another form of corrosion that takes place when two different metals are in contact. The presence of water with the two different metals allows corrosion to take place due to the galvanic cell action, as displayed in Figure 2. The rate of this kind of corrosion is determined by the amount of contaminants in the circulating water (Piper, 1999). Galvanic corrosion occurs only if the following conditions are met:

a) Two different metals must be present
b) The two metals must be in contact, or an electrically conductive path between the two must be present

c) There must be an electrically conductive path for the ions to move from the "anode" to the "cathode"

If any of these conditions is not satisfied, galvanic corrosion is not likely to take place (Galvanic Compatability Corrosion Dissimilar Metal Corrosion). The different metals react differently and have a different corrosion potential under different environments. The metal with the most positive corrosion potential then acts as the cathode, and the one with the more negative corrosion potential becomes the anode. The coupling of the metals causes the cathode to reduce its corrosion rate, and the anode to increase its corrosion rate. Therefore, this technique is used as means of cathodic protection from corrosion. An example could include the corrosion of iron coupled with copper steel or stainless steel fittings (Beavers and Thompson, 2006).

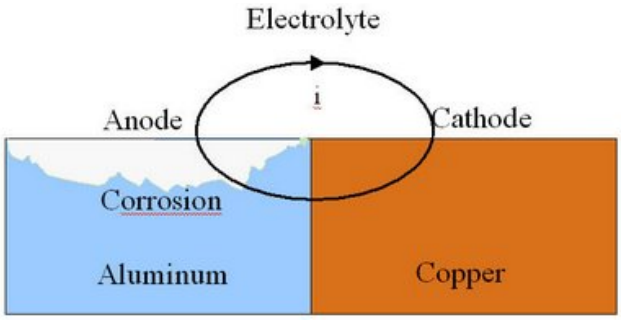

Figure 2: Galvanized Corrosion Process (Corrosion Between Anodized Aluminum and Steel, 2009)

2.5 Crevice Corrosion

Crevice corrosion refers to the localized corrosion that occurs at the crevice or gap between two or more joining metals (or non-metals in some cases), such as in flanges, and a stagnant solution exists. The damage takes place due to the difference in constituents' concentration, mainly oxygen, in the surfaces involved (Rashidi, Alavi-Soltani and Asmatulu, 2007).

2.6 Concentration Cell Corrosion

Concentration cell corrosion is a type of galvanic corrosion that occurs when the same metal is exposed to different corrosive environments. The difference in the environment causes the metal to develop an anodic region and a cathodic region. The electrolyte and the metallic path complete the circuit and cause the electrochemical reaction to start taking place. This type of corrosion is illustrated in the Figure 3 (US Department of Defense, 2003).

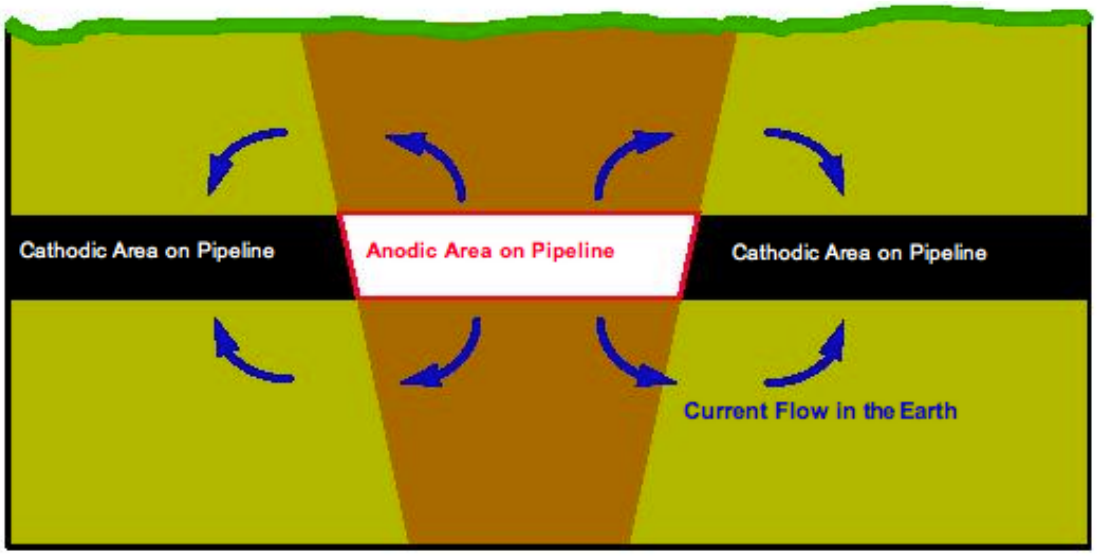

Figure 3: Concentration Cell Corrosion in a Pipeline Underground (US Department of Defense, 2003)

2.7 Corrosion Under Insulation

Corrosion Under Insulation (CUI) is a main concern for modern plants. CUI refers to the external corrosion that takes place underneath the jacketed thermal insulation on pipes and vessels. The problem with this kind of corrosion is that it is often of the pitting kind and is localized in areas that are not detected directly by inspection programs. This is especially hazardous when the insulation covers it until it reaches severe levels that truly threaten the life of the pipe/vessel. This form of corrosion will be discussed more thoroughly in a later chapter (Twomey, 1997).

2.8 Erosion/Corrosion

Erosion/corrosion is a very complex type of material loss that involves both electrochemical and mechanical processes. This type of corrosion can affect the lifetime of the component dramatically, because not only does it damage the thin passive film on the surface of the material, but also the base metal (Barker, et al., 2011). Erosion/corrosion will also be discussed in more details in a later chapter.

2.9 Microbially-Induced Corrosion

Microbially-induced corrosion, from the name, is the type of corrosion induced by the existence of microorganisms, including bacteria and fungi. While the microorganisms do not cause the corrosion damage per se, their by-products promote different types of corrosion by interacting with the corrosion products and accelerating the corrosion process. The attack can be caused by aerobic or anaerobic bacteria, but is most serious when different kinds of bacteria exist. Under these conditions, the bacteria act cooperatively to coexist and produce an environment favorable to the growth of all existing species. For example, anaerobic bacteria, which are the type of bacteria that survives only in the absence of oxygen, can exist in aerobic conditions if they live beneath deposits or films where aerobic bacteria consume the oxygen, as shown in Figure 4.

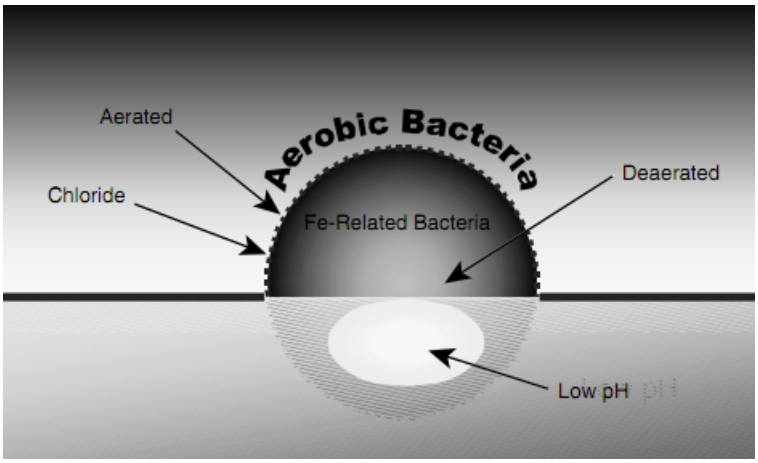

Figure 4: Anaerobic Bacteria Coexisting with Aerobic Bacteria (Beavers and Thompson, 2006)

Studying this type of corrosion requires understanding the microbiology that is taking place in relation to corrosion. However, its presence has been problematic in many industries including the petrochemical, marine, power, aircraft, water supply and distribution, and process industries. A study found that about 20-30% of external corrosion in underground pipelines is related to microbially-induced corrosion (Al-Darbi, et al., 2002) (Beavers and Thompson, 2006).

3. AVAILABLE METHODS OF INSPECTION

3.1 Introduction

Over the past decades, many methods of inspection have been developed for detecting and monitoring the various forms of corrosion. Some inspection methods are more effective than others, but are not as time or cost effective. An effective corrosion detection technique should be capable of detecting corrosion in any location and under different conditions, and it should be capable of providing reliable, accurate data. It should also have rapid response in order to allow for solutions for severe problems to be studied and implemented immediately. Moreover, it should be sensitive enough to detect actual minor flaws in order to make sure corrosion damage as early as possible and ensure that the necessary measures are taken before it is too late. Finally, corrosion detection techniques should be cost-effective. Several inspection methods need to be implemented in order to detect the various forms of corrosion. The most common methods of inspection include: visual inspection, ultrasonic and acoustic methods, radiographic methods, thermal inspection, electromagnetic inspection, electrical resistance methods, electrochemical methods, electrochemical noise, electrochemical impedance spectroscopy, chemical sensors, and others. Some of these methods will be discussed in this chapter (Agarwala, Reed and Ahmad, 2000).

3.2 Visual Inspection

Visual inspection is and has always been the primary and most effective corrosion inspection method, but it is also the most costly in terms of money and time. It involves periodic visual testing of the exterior of the equipment and pipes for leaks, distortion, or any evidence of internal damage or physical change. Visual inspection requires good vision, adequate lighting, and familiarity and understanding of what is being investigated. Magnifying glasses may be used in order to enhance the inspection effectiveness. Visual inspection may be conducted through sentry holes, borescopes, or charged couple devices. Sentry holes are holes that are drilled on the external surface of the equipment at locations where corrosion is most likely to occur. The holes are drilled to a depth corresponding to the design wall thickness of the vessel of pipe minus the permissible corrosion allowance that is usually included in the design. When corrosion starts consuming the allowance thickness, a small leak starts developing on the surface of the equipment, which provides a timely warning of the need for maintenance. The holes are threaded in order to provide temporary plugging until a shutdown is possible (Howard, Gibbs and Elder, 2003) (Agarwala, Reed and Ahmad, 2000).

Borescope is an optical device that consists of a tube with an eyepiece at one end equipped with a light source. The tube may be flexible of rigid depending on the application and the eyepiece allows for visual on-stream inspection of the internal

surfaces of the equipment of piping. This device makes it possible to inspect inaccessible points without disassembling the equipment, and may be used in holes or openings of 3 mm of greater in diameter. The principal of the borescope is shown in Figure 5.

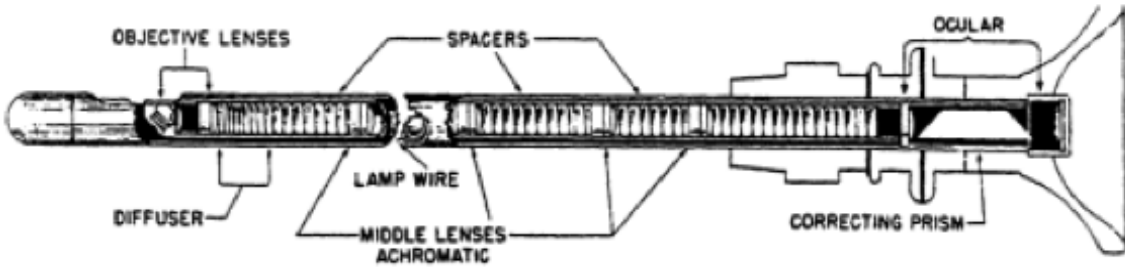

Figure 5: Borescope (Chawla and Gupta, 1993)

Charge Coupled Devices (CCD) are also optical scanning devices that include techniques such as edge of light, optical profilometry, and video imaging. These devices use CCD cameras to take and record images, which are then processed through computer-based methodologies to detect flaws on the surface. This technique is very effective in detecting and classifying the type of damage. Moreover, CCD devices are typically relatively cheap and may be used to scan large

areas. On the other hand, they lack precision and are labor intensive and may be applied only on open surfaces (Agarwala, Reed and Ahmad, 2000).

3.3 Ultrasonic and Acoustic Inspection

Ultrasonic and Acoustic testing is an inspection technique that has been and still is widely used across the industry. It provides excellent resolution and can detect minute material and thickness losses with a relatively short response time. The main principle here involves utilizing high frequency sound waves above 0.2 MHz to make measurements. Typical ultrasonic and acoustic systems consist of a transducer, a receiver (or a pulser) and a display device. The reflection or pulse echoing shown on the display device allows for flaw detection. The sound energy that is produced by the transducer propagates through the cross section of the vessel or pipe in the form of waves and when a flaw is detected, part of the energy is reflected back. The transducer then transforms the reflected signal into an electrical signal, which is then displayed on a screen. Figure 6 shows an example of ultrasonic testing acquisition.

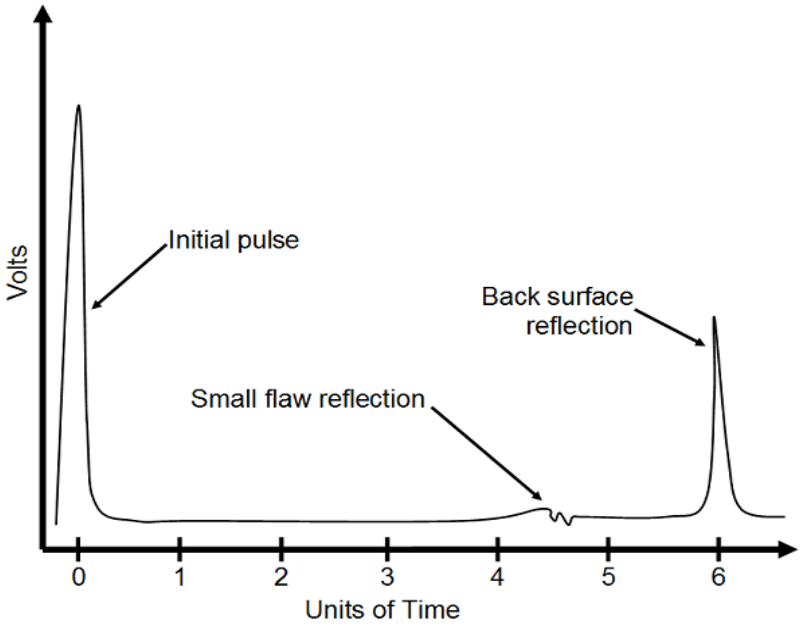

Figure 6: Example of Ultrasonic Testing Acquisition (Ultrasonic Nondestructive Testing -Advanced Concepts and Applications, 2012)

As shown in Figure 6, the reflected signal from the flaw can then be plotted as a function of the time traveled when the echo was received and this travel time can then be related to the distance traveled and the flaw may be located. The echo also gives information about the size of the flaw so the severity of the situation can be estimated (Agarwala, Reed and Ahmad, 2000).

3.4 Radiographic Inspection

Radiographic inspection is another non-destructive testing technique that has been commonly used to monitor corrosion, especially in the petrochemical industry. The radiation type may be neutrons, x-rays, or gamma rays. Radiographic methods have an advantage over other common methods in that they can detect corrosion without the costly removal of the insulation material. However, these methods require radiation safety measures to be taken and they have low sensitivity. Corrosion is detected by measuring the thickness of the cross section of the pipe or vessel. The radiation rays are sent through the cross section of the pipe or vessel and penetrating rays are projected as images on a thin film. The extent of the damage is estimated by comparing the images to those of the undamaged part. An example of radiography inspection results is shown in Figure 7.

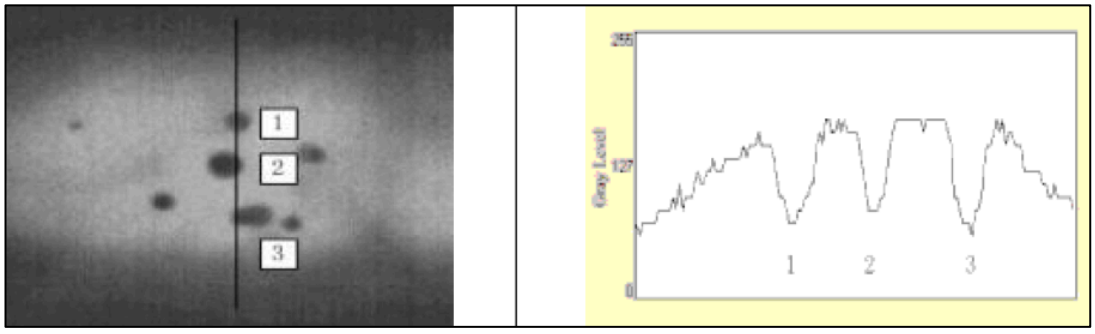

Figure 7: Radiography Results (Wanga and Wong, 2004)

The picture on the left in Figure 7 is the radiographic film obtained from the radiography inspection. This picture is then processed by experienced interpreters, or computer software in order to estimate the extent of the damage and produce a chart as what is shown in the picture on the right (Balasko, et al., 2005) (Agarwala, Reed and Ahmad, 2000).

3.5 Electromagnetic Inspection

There are three main categories of this inspection method: magnetometers and dielectrometers, superconducting quantum interference device, and magnetic flux leakage technique. Magnetometers and dielectrometers are used not only to detect corrosion under paint, but to also detect the damp spots and the depth of moisture in the coating layer. Magnetic fields and inductive coupling are used to plot the conductivity profile of the area being inspected. Reduced conductivity at the metal surface may be caused by reasons other than wall thinning due to corrosion. For example, it may be caused by an oxygen diffusion layer; however, this may be the result of early-stage corrosion.

Superconducting Quantum Interference Device (SQUID) are devices used to carry out quantitative measurements of corrosion rate and material loss with high resolution and sensitivity. These devices are basically magnetometers that are mainly used for very weak magnetic fields because of their high sensitivity. At low

frequency, SQUID eddy current measurements offers phase-sensitive detection that allows a depth selective technique to image material loss within aluminum structures. In many cases, the sensitivity of SQUIDs makes them useful when other methods fail to make sensible measurements (Fagaly, 2006) (Agarwala, Reed and Ahmad, 2000).

Magnetic Flux Leakage Technique is another approach to monitoring corrosion in pipelines while in-service. Smart pigs that employ this technique are the most cost-effective approach out of all in-service corrosion inspection methods. However, this technique is not useful for pipes with smaller diameters, and therefore its usability is limited to larger pipes and transmission lines (Agarwala, Reed and Ahmad, 2000).

Generally speaking, numerous methods of inspection for corrosion exist. Some are more effective than others, some are more costly than others, and some are only useful to some extent or under particular conditions. Therefore, depending on the application, the most appropriate method of inspection is chosen.

4. CORROSION UNDER INSULATION AND METHODS OF DETECTING IT

4.1 History

Corrosion under insulation (CUI) has become a serious threat to many of modern plants. It started receiving a great amount of attention in petroleum refineries, chemical plants, power generating plants and other facilities in the 1980s. The reason being that the insulation which had previously been used at locations of 300 ^{o}F and above started being used at much lower temperatures ~200 ^{o}F after the first oil crisis in 1973 (Tada, Suetsugu and Mori, 2010). Being localized and hidden by the insulation, it typically causes failures in areas that are not of primary concern to the maintenance program. Not only does it often result in catastrophes, but it always has a strong economic effect in terms of time and money. CUI is especially problematic in carbon steels and 300 series stainless steels. On carbon steels, it is usually either of the generalized or the localized nature. However, in stainless steels, it is more often than not pitting corrosion induced stress corrosion cracking.

The main factor to corrosion under insulation, like most other corrosion forms, is oxygen combined with moisture. However, in this case, the insulation material, which acts as a sponge that entraps the moisture, might increase the severity of the resulting damage, by not allowing the moisture to evaporate and also buy acting as a carrier that helps the moisture spread from one spot to others. Moreover, traditional thermal insulation materials may contain chlorides, which upon

exposure to moisture may be released into the moisture layer on the surface of the metal and cause pitting corrosion or stress corrosion cracking. The source of the water can be rain, leakage, deluge system, wash water, or sweating from the process temperature. CUI can occur at a wide range of temperatures; however, it is more significant at temperatures between 32 and 300 ^{o}F, especially at about 200 ^{o}F. The following five areas are specified by API 570 as susceptible to CUI:

1. Areas exposed to mist from cooling water towers
2. Areas exposed to steam
3. Areas exposed to deluge systems
4. Areas subject spills, moisture, or acid vapors
5. Carbon steel piping insulated for personnel protection operating between 25 and 250 ^{o}F.

Many other areas of the process are also susceptible to CUI, including deadlegs that operate at a different temperature from the active line. All of these areas are prone to water ingress and therefore must receive special attention.

It is difficult to calculate the direct costs of corrosion under insulation. However, a study that was conducted by ExxonMobil and presented in 2003 showed that the corrosion under insulation, rather than process corrosion, is responsible for the highest incidence of leaks in the refining and chemical industries. The study also

showed that corrosion under insulation is responsible for about 40-60% of piping maintenance costs (Industrial Nanotech, Inc., 2006).

4.2 Problems with Methods of Inspection

Some of the most commonly used methods of detection of CUI include visual inspection (insulation removal), profile radiography, ultrasonic thickness measurement, real time radiography, and pulsed eddy current testing. Each one of these methods has some shortcomings that make it either inapplicable under some conditions, or not accurate enough in detecting corrosion under insulation. Visual inspection is still the preferred method in many facilities today, because it is very effective. This method, however, is very costly in terms of money and time lost. It requires the insulation to be peeled off the entire surface of the metal, the surface condition to be checked, and finally the insulation to be replaced. If the insulation is removed while the piping is in service, many process related problems may occur. The following table summarizes some of the specifications as well as the advantages and disadvantages that the other four methods have (Callister, 1972) (Tada, Suetsugu and Mori, 2010).

Table 1: Comparison of the Most Commonly Used Methods of Detection of CUI

Method	Profile Radiography	Ultrasonic Measurement	Real-Time Radiography	Pulsed Eddy Current
Influence of internal fluid	Yes	Yes	Yes	No
Inspection of Long Distance	Not applicable	Applicable	Not applicable	Not applicable
Removal of Insulations	No need	Need	No need	No need (less than 80 mm in thickness)
Corrosion can be detected	Corrosion, erosion and the accumulation of deposits	Localized corrosion (10% depth level of sectional area)	Localized corrosion	General corrosion like concave
Inspection accuracy	Reasonably good	Not good	Good	Not good
Safety Concerns	Radiation		Radiation	

As shown in Table 1, each of the main NDT methods used for the detection of CUI has its own drawbacks. Ultrasonic may have a very high inspection speed, however, it may not be used for all pipe configurations and it requires some of the insulation to be removed, and it does not have very high accuracy. Radiography methods provide accurate results, but there are some safety implications with the radiation that they require. Pulsed eddy current testing only gives relative results and works better with flatter objects (Wassink, 2008).

4.3 Objective

A different non-destructive technique of detection of corrosion under insulation that does not require the insulation to be removed needs to be investigated. This method is needed to overcome at least some of the shortcomings shown by the commercial NDT methods currently used. Also this method needs to be safe, accurate, fast, reliable, and adaptable.

4.4 X-Ray Computed Tomography

To meet the objective of this research, many approaches were considered and a number of methods were studied, particularly electrical computed tomography and X-ray computed tomography. However, based on the results of some preliminary experiments, it was found that electrical computed tomography would not serve the purpose of this project. It was found that the metal surface of the pipe would block the signals from the tomography system, and interference with internal conductive fluids is possible. Moreover, the insulation material, especially dry insulation, would not allow the AC current to pass through. Therefore, electrical tomography was left out of the possible methods to be investigated and X-ray computed tomography was selected for further studies.

X-ray tomography is a non-destructive technique that is used to visualize the inside of opaque objects. This method has been commonly used in the medical profession in CT and CAT scanners. It has also been used recently in civil engineering to monitor corrosion in steel reinforcement in concrete (Beck, et al., 2010).

In X-ray tomography, the specimen is placed between the X-ray source and a detector. The detector determines the intensity of the X-rays after leaving the specimen, which is then compared to the initial intensity of the X-rays leaving the source, and based on that, the density of the material is determined. The density distribution of the specimen is then calculated and an image is created with each density level assigned a color (Advanced Characterization of Infrastructure Materials Laboratory, 2009). This is done while the object is being rotated 360^{o} in order to capture the density of the cross section of the object from all angles.

4.4.1 X-Ray Computed Tomography vs. Real Time Radiography

While similar to real-time radiography, X-ray tomography seems to be a better fit for the purpose of this work. It is different from real-time radiography, in that it is mainly used to perform tomographic reconstructions of static material distribution and has the ability to determine the material distribution on the outside and inside of the material. This can be used to investigate both internal and external corrosion simultaneously. On the other hand, real-time radiography provides an X-ray "shadow" of flaws in the specimen, which is not as clear as the image provided by X-

ray computed tomography (Torczynski, et al., 1997). Moreover, X-ray tomography provides a 3-D image of the specimen while real time radiography provides a 2D image, which allows for more accurate inspection of the object. Finally, X-ray tomography has shown more accurate results than real time radiography in medical applications (Carreon, et al., 2008).

4.5 Experimental Approach

In order to understand whether X-ray tomography would be a good option for corrosion detection, it was necessary to know first to what extent the system can detect small flaws in an object. This is important in order to make sure the system is capable of detecting any minor corrosion taking place, even if it is of low severity. After that, it was necessary to determine whether the results of the system are affected by the insulation jacketed around the exterior of the pipe. This is important in order to know whether the insulation would need to be removed for the system to be used for corrosion inspection. Finally, it was of interest to test whether the system was useful for detecting internal corrosion as well.

4.5.1 Experiment 1: The Accuracy of the X-Ray Tomography System

To test the system for detecting small flaws, three small holes of different sizes (0.442”, 0.315”, and 0.126”) were drilled along the same cross section of a 4” carbon steel pipe, as shown in Figure 8. The system was used to take multiple scans

at different locations of the cross sections where the holes were drilled. The locations where the scans were taken are indicated with the thin red lines shown in Figure 9. The 2-D images were then assembled on top of one another via computer imaging and the 3-D volume of the pipe was reconstructed on Vizio®. The results of this analysis will be discussed in section 4.6.1

Figure 8: Holes Drilled on the Same Cross-Section of a Pipe

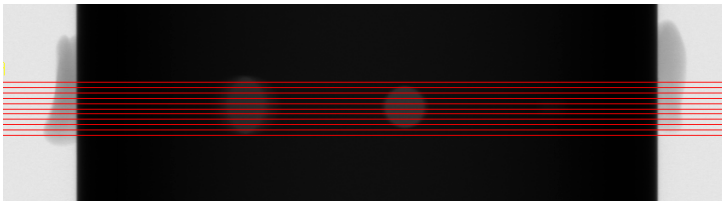

Figure 9: Locations Where X-Ray Scans Were Taken

4.5.2 Experiment 2: The Effect of the Insulation Material on the Output

Three main types of insulation of different densities were tested in this experiment: high-density foam, low-density foam, and fiberglass. The three insulation materials were jacketed around the same pipe, each at a time, and scans of the same cross-sections were taken each time. The insulation was wrapped around the pipe with aluminum casing to test whether that could affect the X-rays penetration through the pipe. Figure 10 shows the three insulation materials that were used for this experiment. The results of this experiment are analyzed in section 4.6.2.

Figure 10: Three Insulation Materials Used

4.5.3 Experiment 3: Is Internal Corrosion Detected?

X-ray computed tomography outdid real time radiography because of its ability to inspect the interior and exterior of an object simultaneously. The 3-dimensional output of the system allows for locating exactly where a flaw might be located. Therefore, it was of interest to see whether this capability could be used for detecting minor internal corrosion in a pipe. A 0.5" pipe with a layer of galvanized corrosion was inspected using the system. Scans at different locations were taken to capture internal corrosion of different severity levels. The results of this section are shown in section 4.6.3.

4.6 Results and Discussion

4.6.1 Experiment 1: The Accuracy of the X-Ray Tomography System

First, 2-D scans were taken of the cross-section where the three holes were drilled on the surface of the pipe. The following figure shows ten of the 2-D scans that were taken, in the order from top to bottom.

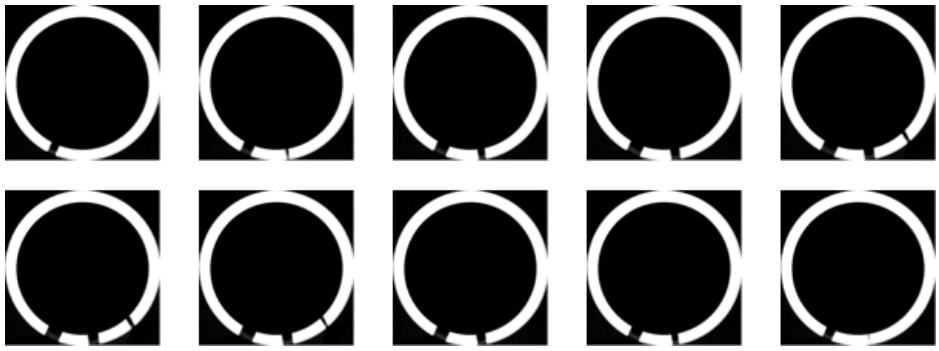

Figure 11: 2-D Scans of the Pipe Cross Section As Displayed on Computer Screen

As clear from Figure 11, the holes in the cross section of the pipe are very clearly shown on the images taken by the system. These images were then assembled on top of one another using Vizio and the 3-D volume, shown in Figure 12, was reconstructed.

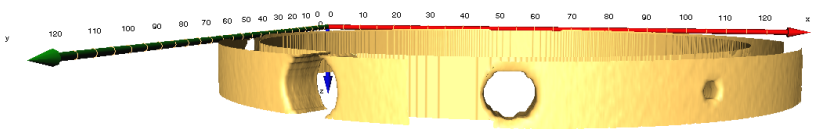

Figure 12: 3-D Image of the Pipe Reconstructed on the Computer

As shown in Figure 12, the three holes were detected very accurately by the system. However, while the holes are perfectly circular in the real pipe, they are not as perfect in the X-ray output. More 2D slices would have to be taken in order to obtain a more accurate result. Moreover, depending on the application, 2D imaging might be sufficient for corrosion (both internal and external) detection, and constructing the 3D volume would be needed only after corrosion damage has been detected and better visualization would be required in order to see how severe the damage is. However, many scans would have to be taken in order to ensure that minor flaws are detected.

4.6.2 Experiment 2: The Effect of the Insulation Material on the Output

As mentioned before, the three types of insulation that were studied here were: high-density foam, low-density foam, and fiberglass. The pipe around which the insulation materials were jacketed was 0.5" in diameter, and the scans were taken at the same of location each time. Figure 13 shows the scans of the same cross section with the different insulation materials.

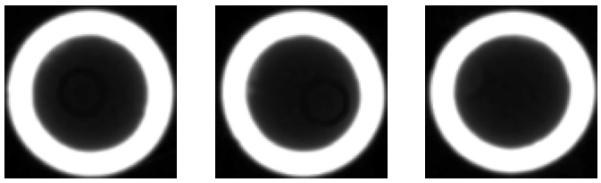

(a) (b) (c)

Figure 13: Cross-Section of Pipe as viewed with Different Insulation Materials Jacketed around it (a) High-Density Foam (b) Low-Density Foam (c) Fiberglass

As shown in Figure 13, the insulation material does not affect the accuracy of the results at all, as the three figures are identical. Also, since the density of the insulation materials is negligible compared to that of the metal surface, the insulation was not visible by any means in the images taken by the system.

4.6.3 Experiment 3: Is Internal Corrosion Detected?

Finally, the system was tested for its ability in detecting internal corrosion. A small pipe with some galvanized internal corrosion that had formed on its surface was used. The following figure shows three images of the corroded pipe. Image 1 was taken at the end of the pipe, Image 2 was taken 2 mm away, and Image 3 was taken 2 mm away from Image 2.

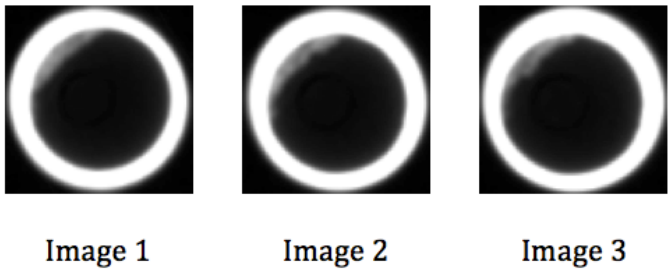

Figure 14: Images of Three Internally-Corroded Cross-Sections of a Pipe

As clear from Figure 14, since the corrosion is of much lower density than the pipe surface itself, the shade of grey that the X-ray tomography system has assigned it is much darker than that of the pipe. However, the system was still successful in detecting the minor corrosion that had formed.

4.7 Conclusion

All in all, X-ray tomography gave accurate results and could be used for corrosion detection. Nevertheless, more research is required to achieve faster scan time to make the method more feasible for large-scale plants. Moreover, it is important to study the mobility of the system and its applicability with respect to investigating multiple pipes at the same time, in order to make sure it would be useful in congested plant areas.

The X-ray computed tomography system used in this study was not portable and cannot be used for on-site inspections. It was only used here because it met the purpose of this study which was to investigate if this method detects corrosion, and to what extent. However, for real life applications, it is recommended that the portable version of this system be used instead. The portable X-ray computed tomography that has been developed recently is known as the TomoCAR, which stands for “Tomographical Computer-Aided Radiography”. The operating principal of TomoCAR, shown in Figure 15, is very similar to that of the classic system.

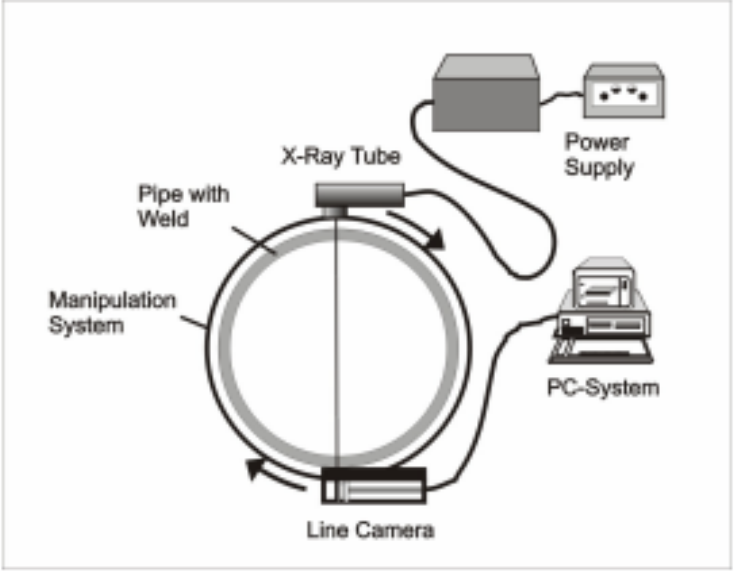

Figure 15: TomoCAR Principal (Redmer, Ewert and Neundorf, 2007)

As shown in Figure 15, here the X-ray source and the screen are mounted on a pipe in parallel facing each other, in order to allow for movement of the x-ray system for scanning of different spots, without affecting the accuracy of the results. In addition, the line camera (screen) that is mounted in front of the X-ray source acts as a radiation collector that reduces any scattered radiation to a very negligible intensity. This system should be investigated in order to ensure that the radiation would not have any negative effects on the users of the system in the long run (Redmer, Ewert and Neundorf, 2007).

5. USING CFD TO STUDY EROSION/CORROSION

5.1 History

Erosion/corrosion, as described earlier, is the acceleration in the rate of corrosion that occurs after the protective film (usually oxide layer) on the surface has been removed via chemical or mechanical processes. The protective film slows down the corrosion process by forming a barrier between the surface of the metal and the corrosive environment. The removal of the surface protective film via chemical processes is usually referred to as flow accelerated corrosion, a term that is more often than not used to refer to erosion/corrosion. Flow accelerated corrosion is a single-phase process that takes place when the protective film is simply dissolved into the solution by the corrosive species. Erosion/corrosion, however, is a mechanical process that involves removing the protective film off the surface by a physical force. In a single-phase flow, this physical force may be caused by the shear stress imposed on the wall by the flow, in other words, the wall shear stress. In a two-phase flow (e.g. fluid containing solid particles, such as sand), the dispersed phase can remove the protective film by an erosive process, affecting not just the protective film, but also the metal underneath.

Erosion/corrosion is a commonly encountered problem and a major concern in many industries, including transportation, power generation, and the petrochemical industry. In the oil and gas industry, it is especially a problem at the

stages involved before the oil or gas is processed at refineries, when it still contains many impurities of different natures, including sand and water, the combination of which provides a very encouraging environment for erosion/corrosion to take place.

Erosion/corrosion has been the root cause of many severe incidents and great losses in terms of lives and money. One of the rather recent large-scale incidents caused by erosion/corrosion is the Mihama power plant explosion that took place in Japan in 2004. The incident occurred when the piping system in a pressurized water reactor led to a steam eruption. First, a fire alarm sounded, alerting the operators at the control room that there was a leak. The operators suspected that steam or hot water started leaking from the piping, and therefore began an emergency load reduction process. Shortly as they were carrying out this process, the reactor tripped automatically and a rupture occurred in a 22" pipe in the condensate system. The incident caused five worker fatalities and six injuries. Later on, investigations determined that the cause of the pipe rupture was in fact erosion/corrosion that had reduced the thickness of the wall of the pipe from 0.39" to about 0.02" (United States Nuclear Regulatory Commission Office of Nuclear Reactor Regulation, 2006).

Another major incident that was caused by erosion/corrosion is the Humber Refinery incident of 2001 that occurred in South Killingholme, United Kingdom. A

drastic failure in the piping in the saturate gas plant released about 397,000 pounds of flammable liquids and gases that ignited causing an explosion and a fire about 20 seconds later. The explosion that threw three people about 570 feet away off their feet caused severe damage to buildings up to 1,300 feet away from the explosion source. The catastrophic incident had the potential to cause fatalities, but fortunately it did not because it occurred when very few people were on site because of shift changeover and surrounding businesses had taken the day off since it was Easter Sunday. Investigations found that the primary cause of the explosion was severe erosion/corrosion of a 6" pipe that had reduced the wall thickness of the pipe from 0.3" to about 0.01", that it could not withstand the internal pressure of the flow (Health and Safety Executive, 2001).

5.2 Factors Affecting Erosion/Corrosion

Many methods have been developed and used for detecting and monitoring erosion/corrosion. However, once the damage starts taking place, it can go at extreme rates and threaten the integrity of the pipes and vessels before the inspection detects it. The main problem with erosion/corrosion is the complexity of the process that is not clearly understood. It is not described by a simple chemical reaction or physical wear. It can be a combination of both, and is affected by many factors related to the flow inside of the pipe; not only the flow material and

operating conditions, but also a single-phase flow would have different erosion/corrosion locations from a two-phase flow, as shown in Figure 16.

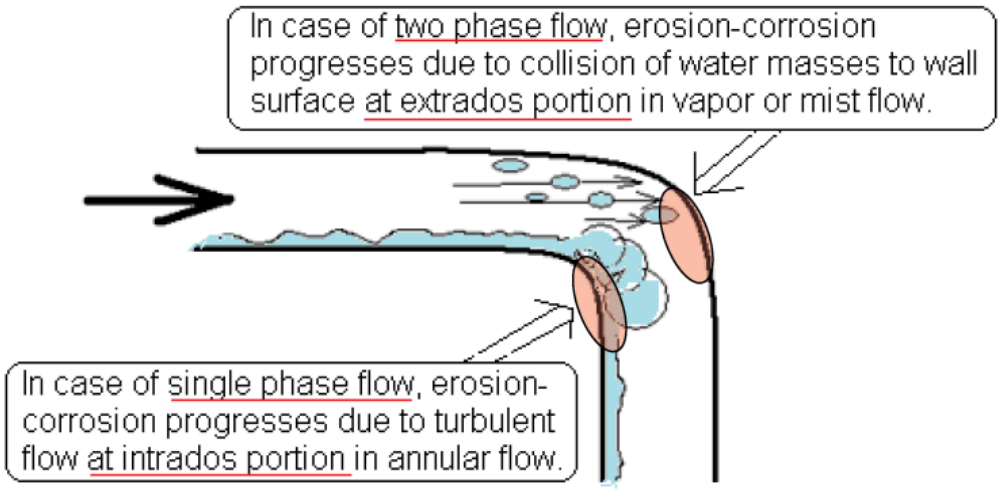

Figure 16: Locations of Corrosion Based on Type of Flow (ClassNK, 2008)

In addition, erosion/corrosion is not only affected by the type of flow inside the pipe, but also the material and geometry of the pipe itself. Some materials are more prone to erosion/corrosion than others, and therefore, may allow the reaction to take place at different rates. Also some pipe geometries might encourage erosion/corrosion more than others, because the geometry of the pipe affects the

flow turbulence, which then imposes different values of stress on different parts of the walls, and hence lead to different erosion/corrosion rates.

The following list includes some of the main factors that affect the rate of erosion/corrosion:

- Flow velocity
- Flow pH
- Flow oxygen content
- Flow temperature
- Pipe shape and geometry
- Pipe material composition

5.2.1 Effect of Flow Velocity on Erosion/Corrosion Rate

Flow velocity is a very important factor in determining the rate of erosion/corrosion. Typically, the higher the velocity, the higher the erosion/corrosion likelihood and that is because as the velocity of the flow increases, the turbulence does as well. At low flow velocities, the corrosion process is more dominant than erosion, but as the velocity increases, erosion starts accompanying corrosion, increasing the rate and extent of the damage. However, after a certain point, any further increase in the flow velocity leads to a lower rate of erosion/corrosion, as shown in the following figure (Ferng and Lin, 2010) (Bush, 1990). Ferng and Lin (2010) explained that the reason for this decreasing trend is

that at high velocities and turbulence, the total metal loss rate can be determined by the chemical reaction rate constant and the metal concentration difference. The reaction rate constant is not really related to the hydrodynamic factors, but the concentration of the metal (or the Fe^{2+}) is strongly associated with the turbulence of fluid inside the piping, and as the mixing increases it also increases, leading to a lower erosion-corrosion rate.

5.2.2 Effect of Flow pH on Erosion/Corrosion Rate

The chemical reaction portion of the erosion/corrosion process is highly affected by the chemical condition of the flow, particularly its pH. It was found that as the pH of the solution goes above 8-9, the rate of erosion/corrosion starts decreasing gradually. The rate of erosion-corrosion tends to drop dramatically when the pH is above 9.2-9.3. It is recommended that the process pH be maintained between 9.3-9.6 (Chawla and Gupta, 1993) (ClassNK, 2008).

5.2.3 Effect of Flow Oxygen Content on Erosion/Corrosion Rate

The amount of oxygen dissolved in the flow inside the pipe is another important factor for determining the rate of erosion/corrosion. Generally, as the amount of dissolved oxygen in the flow decreases, the erosion/corrosion rate increases. If the oxygen concentration drops below 200 ppb, the rate of erosion/corrosion increases significantly. This trend is represented in Figure 17.

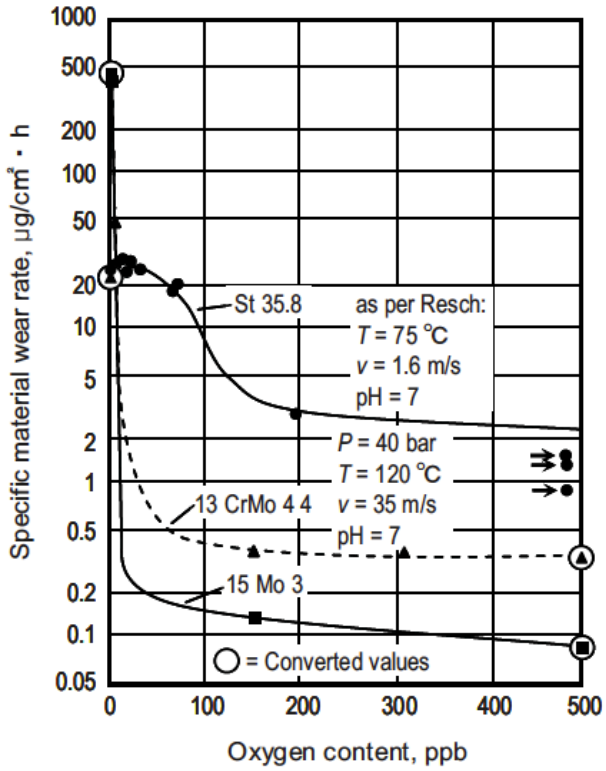

Figure 17: The Relationship between Erosion/Corrosion Rate and Dissolved Oxygen Concentration for Different Pipe Materials (ClassNK, 2008)

5.2.4 Effect of Temperature on Erosion/Corrosion Rate

The rate of erosion/corrosion is also affected by the temperature of the process. Temperatures within the range ~250 °F (121 °C) to ~400 °F (204 °C) tend to increase the rate of the wall thinning due to erosion/corrosion. For a single-phase flow, the rate reaches maximum at around 275 °F (135 °C) for a single-phase flow and about 356 °F (180 °C) for a two-phase flow. However, these values are different

for pipes with different metal surface composition. This will be discussed in section 5.2.6. The following graph displays the relationship between the rate of erosion/corrosion rate due to flow accelerated corrosion and the temperature for different pipe materials.

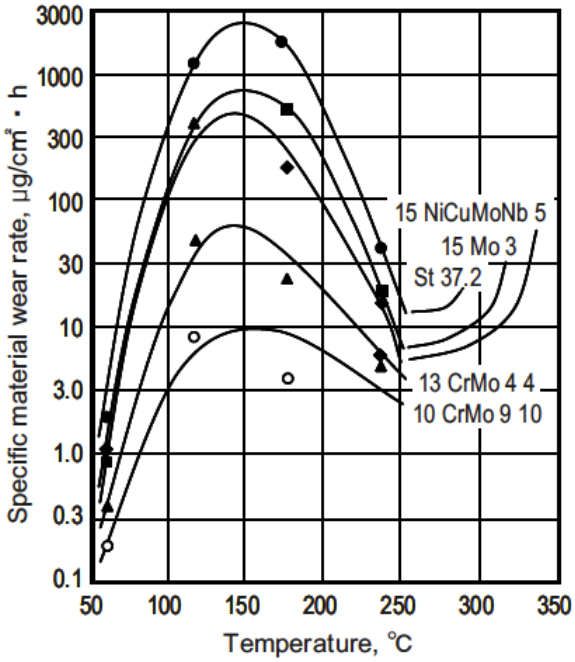

Figure 18: Relationship between Erosion/Corrosion Rate and Temperature (ClassNK, 2008)

As shown in Figure 18, the relationship between the erosion/corrosion rate and the temperature has a convex shape with a maximum point and decreases on both sides farther from the maximum (ClassNK, 2008).

5.2.5 Effect of Pipe Geometry on Erosion/Corrosion Rate

The geometry of the pipe is essential in determining the corrosion rate. A small change in a pipe geometry or orientation can drastically change the flow complexity inside causing different values of turbulence, which in turn affects the rate of erosion/corrosion. Generally, turbulence is generated in pipefittings, behind orifices or valves, at T-sections, at bends and elbows, as well as at diffusers and reducers. For this reason, those are the areas that are usually most susceptible to erosion/corrosion in pipes. Another reason is that the erosion/corrosion process is further encouraged by water, which different geometries might cause it to accumulate in certain spots, such as at bend areas and T-junctions (ClassNK, 2008).

5.2.6 Effect of Pipe Material on Erosion/Corrosion Rate

Finally, the pipe material plays an important role in determining the erosion/corrosion rate. The composition of the pipe material determines the nature of the protective film that forms on the surface and slows down the damage process. When a continuous, dense, solid film forms over the metal surface, better protection against erosion/corrosion is provided and the rate of attack decreases. Stainless steel is considered one of the most corrosion-resistant materials because it has the ability to form a very strong passive film that can withstand any oxidizing

conditions (Chawla and Gupta, 1993). Some of the main components that may be added to the metal composition to increase its corrosion-resistance include chromium, copper and molybdenum (Bush, 1990).

5.3 Objective

In this work, computational fluid dynamics tools were implemented in order to study the effect of some of the flow hydrodynamic factors on the erosion/corrosion rate. The main purpose of this technique was to understand how the different hydrodynamic parameters affect the erosion/corrosion rate. This, in turn, would allow for determining where erosion/corrosion would take place before it occurs by simply entering the properties of the flow on the computer. Not only would this technique allow for determining erosion/corrosion sites before it starts taking place, but it would also give an indication of how much erosion/corrosion would take place, before it is too late and an incident occurs. In other words, it would help mechanical integrity staff make predictions while scheduling maintenance services.

5.4 Computational Fluid Dynamics and Erosion/Corrosion Modeling

Computational Fluid Dynamics (CFD) is a fluid mechanics technique that has become widely used in recent years. It is used to predict flow behaviors by applying numerical analysis methods to solve partial differential equations. CFD tools were

first used in the 1940s to predict the behavior of supersonic flows over sharp cones. The applications of CFD have broadened as the technology advanced and more numerical models were available, and CFD has become an essential part of fluid dynamics that builds on with experiments and theory (Wendt, 2009).

Recently, significant amounts of research have been dedicated to study various types of corrosion through CFD modeling. Many studies were investigated but the one that was most relevant was a study that investigated the use of CFD to predict erosion/corrosion in piping systems in pressurized water reactors in power plants. The main hydrodynamic parameter that is investigated in this study was the near-wall turbulent kinetic energy. Here, a conservative model to define the relationship between the wall-thinning rate due to erosion/corrosion to the turbulent kinetic energy was proposed. This relation was found by plotting plant measurements of erosion/corrosion, for different geometries and flow conditions, as a function of the turbulent kinetic energy as predicted by CFD. By plotting the curve of best fit through the data points, as well as the more conservative curve that envelops all the plant measurement point, this relationship was defined. Both of these curves are shown in Figures 19(a) and 19(b).

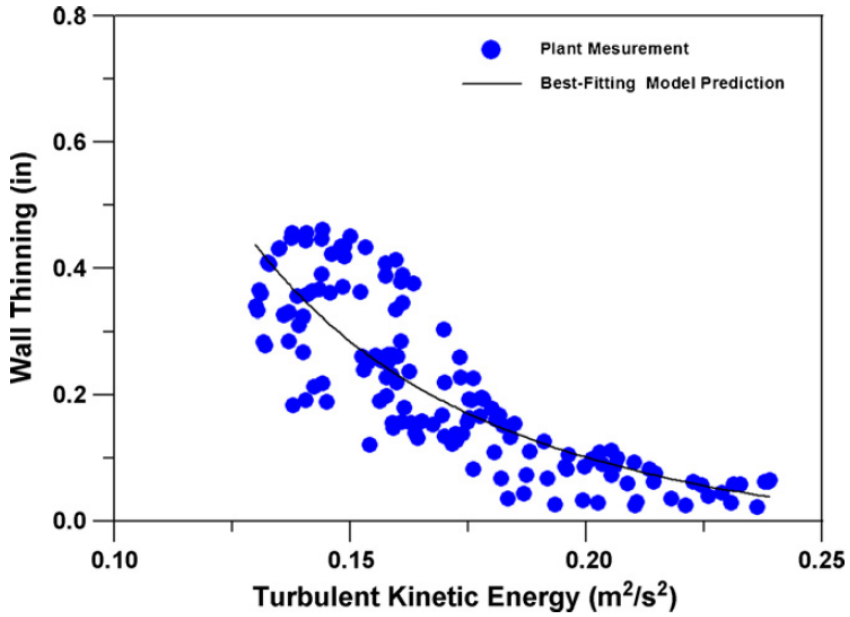

(a)

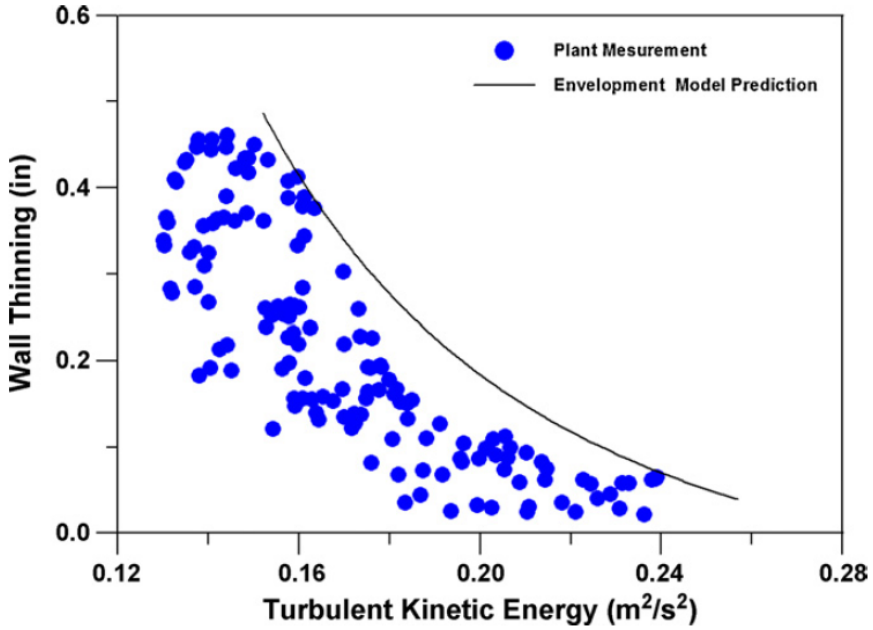

(b)

Figure 19: Relationship Between Wall-Thinning Rate and Turbulent Kinetic Energy (Ferng and Lin, 2010) (a)

As shown in Figure 19, the wall thinning values were decreasing as the turbulent kinetic energy increased. The plant measurements were all taken for the same piping system but at different locations with different turbulent kinetic energy values (Ferng and Lin, 2010). The same approach was used in this research and is explained in the next few paragraphs.

5.5 Approach

ClassNK provided some erosion/corrosion data for a period of 20 years in their report: "Guidelines on Pipe Wall Thinning". The data was for a nuclear power station, where erosion/corrosion has been commonly encountered and has caused several incidents in the past, including the Mihama Nuclear Power Station explosion of 2004. It included data for different geometries, including bends, T-junctions, and valves. It also included different flow conditions for each geometry. The maximum wall thickness loss due to erosion/corrosion was provided for each shape, and the location where it takes place was also specified (ClassNK, 2008). This data was then used to study the relationship between the flow hydrodynamic factors and the rate of erosion/corrosion. The following are the general steps that were carried out to meet the objective of this work:

1. The geometries (discussed later) were built on SolidWorks
2. The meshing of the geometries was formed on Gambit

3. The operating conditions that led to erosion/corrosion were used on FLUENT® to carry out the flow hydrodynamic factors predictions
4. The erosion/corrosion values from the literature were then related to the hydrodynamic flow factors that were predicted by FLUENT®

The main hydrodynamic factors that were considered initially were the surface shear stress and the flow turbulence, both of which are known to affect the rate of erosion/corrosion. However, the results showed that the dynamic pressure plays an important role in the picture, and therefore, it was studied as well.

The simulations were carried out for four of the shapes mentioned in the report, namely: two bends of different elbow radii (R=1.5D and R=3D, where R is the radius of the elbow, and D is the diameter of the pipe), a T-branch, and a merging T-junction. The T-branch and the T-junction had the same geometry, but the direction of the flow inside was different, as shown in Figure 20.

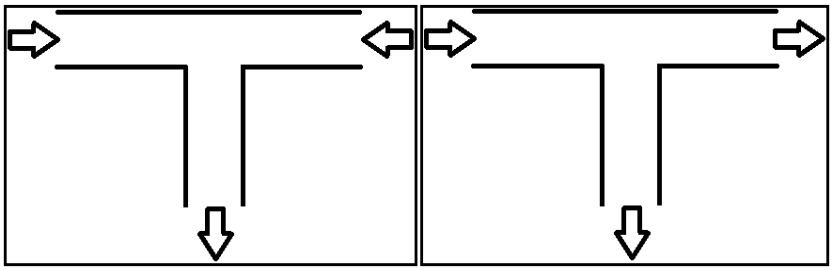

(a) (b)

Figure 20: (a) Merging T-Junction (b) T-Branch

The grids that were used for the four shapes were all hexahedral, which provide more accurate results. Also, the meshes were refined near the walls using Gambit to better capture the behavior of the flow near the walls.

After the meshing of the geometries was completed, the flow conditions from the literature were all input on FLUENT®, and the standard k-ε model was used to predict the flow behavior. This model was chosen because it is the most commonly used model for turbulence calculations. The boundary conditions used in all simulations were mass flow rate at the inlet(s), and pressure at the outlet(s) and only steady state solver was used. The y^+ value, which is a dimensionless number calculated by FLUENT® to indicate how well the behavior of the flow near the wall is captured, was also calculated. Its main purpose is to make sure that the meshes developed by Gambit were fine enough to make accurate predictions by ensuring

that its value is within the range $50<y^{+}<300$, for standard wall function. The y^{+} value is given by the following formula:

$$y^{+} = \frac{\rho C_{\mu}^{1/4} k_p^{1/2} y_p}{\mu} \quad (1)$$

where: p is a node

k_p is the turbulent kinetic energy at the near-wall node p

y_p is the distance from point p to the wall

C_{μ} is a constant for K-epsilon model

ρ is the density

μ is the dynamic viscosity

The standard K-epsilon model is given by the following formulas:

1. Transport equation for turbulent kinetic energy "k":

$$\frac{\partial}{\partial t}(\rho k) + \frac{\partial}{\partial x_i}(\rho k u_i) = \frac{\partial}{\partial x_j}\left[\left(\mu + \frac{\mu_t}{\sigma_k}\right)\frac{\partial k}{\partial x_j}\right] + P_k + P_b - \rho\varepsilon - Y_M + S_k \quad (2)$$

2. Transport equation for turbulent dissipation rate "ε":

$$\frac{\partial}{\partial t}(\rho \varepsilon) + \frac{\partial}{\partial x_i}(\rho \varepsilon u_i) = \frac{\partial}{\partial x_j}\left[\left(\mu + \frac{\mu_t}{\sigma_\varepsilon}\right)\frac{\partial \varepsilon}{\partial x_j}\right] + C_{1\varepsilon}\frac{\varepsilon}{k}(P_k + C_{3\varepsilon}P_b) - C_{2\varepsilon}\rho\frac{\varepsilon^2}{k} + S_\varepsilon \quad (3)$$

3. Turbulent viscosity is modeled as:

$$\mu_t = \rho C_\mu \frac{k^2}{\varepsilon} \quad (4)$$

$$P_k = \mu_t S^2 \quad (5)$$

S is the modulus of the mean rate of strain tensor and given by:

$$S = \sqrt{2 S_{ij} S_{ij}} \quad (6)$$

$$P_b = \beta g_i \frac{\mu_t}{P_{rt}} \frac{\partial T}{\partial x_i} \quad (7)$$

where: P_{rt} is the Prandtl number for energy

g_i is the gravity

β is the coefficient of thermal expansion

For standard models, the default value of $P_{rt} = 0.85$, and β is given by:

$$\beta = -\frac{1}{\rho}\left(\frac{\partial \rho}{\partial T}\right)_p \quad (8)$$

The model constants are given as follows:

$$C_{1\varepsilon} = 1.44 \quad (9)$$

$$C_{2\varepsilon} = 1.92 \quad (10)$$

$$C_{\mu} = 0.09 \quad (11)$$

$$\sigma_k = 1.0 \quad (12)$$

$$\sigma_{\varepsilon} = 1.3 \quad (13)$$

A single-phase flow of water was modeled for the four shapes listed previously. The flow was also modeled at 6 speeds: 0.26, 1.2, 2.4, 2.5, 3.6, and 7.5 m/s. As mentioned previously, both of the flow velocities and the shape of the pipe affect the turbulence of the flow inside the pipe and the shear stress imposed by the flow on the pipe walls. Therefore, studying the same flow in different shapes and at different speeds provides different turbulence and wall shear stress values.

Finally, the results from FLUENT® gave the turbulent kinetic energy and surface shear stress values, as well as other factors, throughout each shape, and this was used to investigate the relationship between the erosion/corrosion and the turbulence and wall shear stress. This was accomplished by plotting the maximum erosion/corrosion value for each shape (obtained from the literature) against the turbulence and wall shear stress at that point of maximum damage (as predicted by FLUENT®).

5.6 Results and Discussion

Figure 21 shows the hexahedral grids that were developed on Gambit for one of the bends as well as the T-junction.

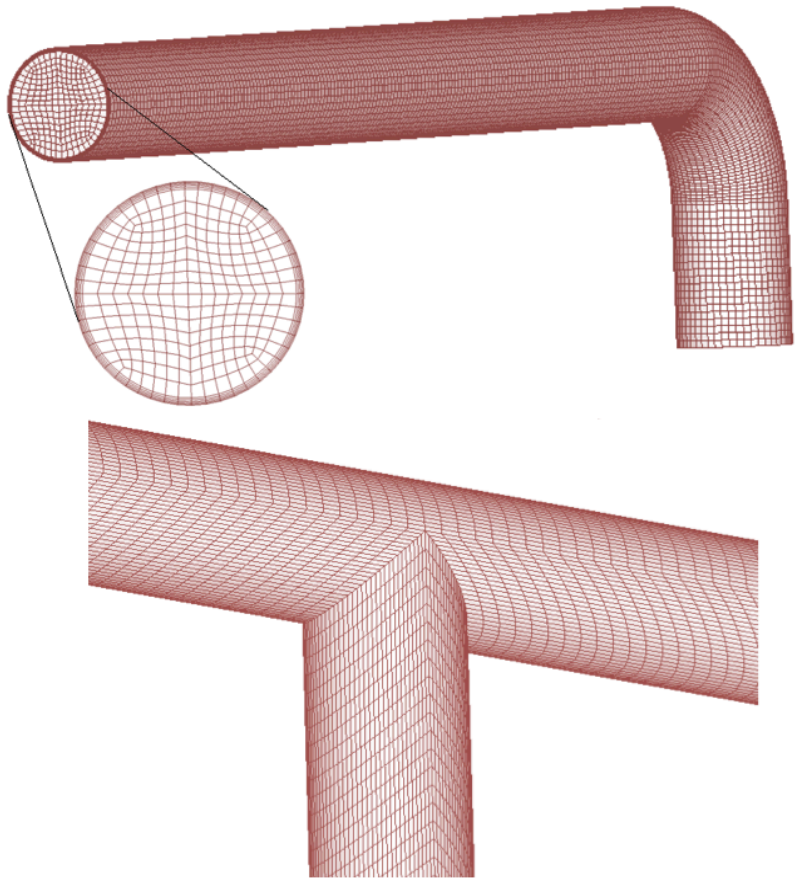

Figure 21: Grids of a Bend and a T-Junction

The cross-section of the pipe bend was blown up in Figure 21 to show how the meshes were refined near the edges in order to visualize more clearly the boundary layer of the flow near the wall. This was necessary in order to obtain more accurate prediction of the hydrodynamic parameters of the flow near the walls of the pipes.

After the grids were completed, the conditions of the flows that led to erosion/corrosion that were collected from the literature were input into FLUENT®, and the model was set up for each of the four geometries considered. The simulations were then left to run under steady state conditions until the solution was complete. After that, the solutions of the simulations were investigated. The results from FLUENT® were obtained in contour plots for a variety of different hydrodynamic factors, with a scale to show the value each color corresponds to, as shown in Figure 22. The main factors that were studied initially were the turbulent kinetic energy and the wall shear stress, both of which were produced by FLUENT®. From contour plots similar to the following (Figure 22), the relationship between erosion/corrosion and factors such as the turbulent kinetic energy and the wall shear stress was studied.

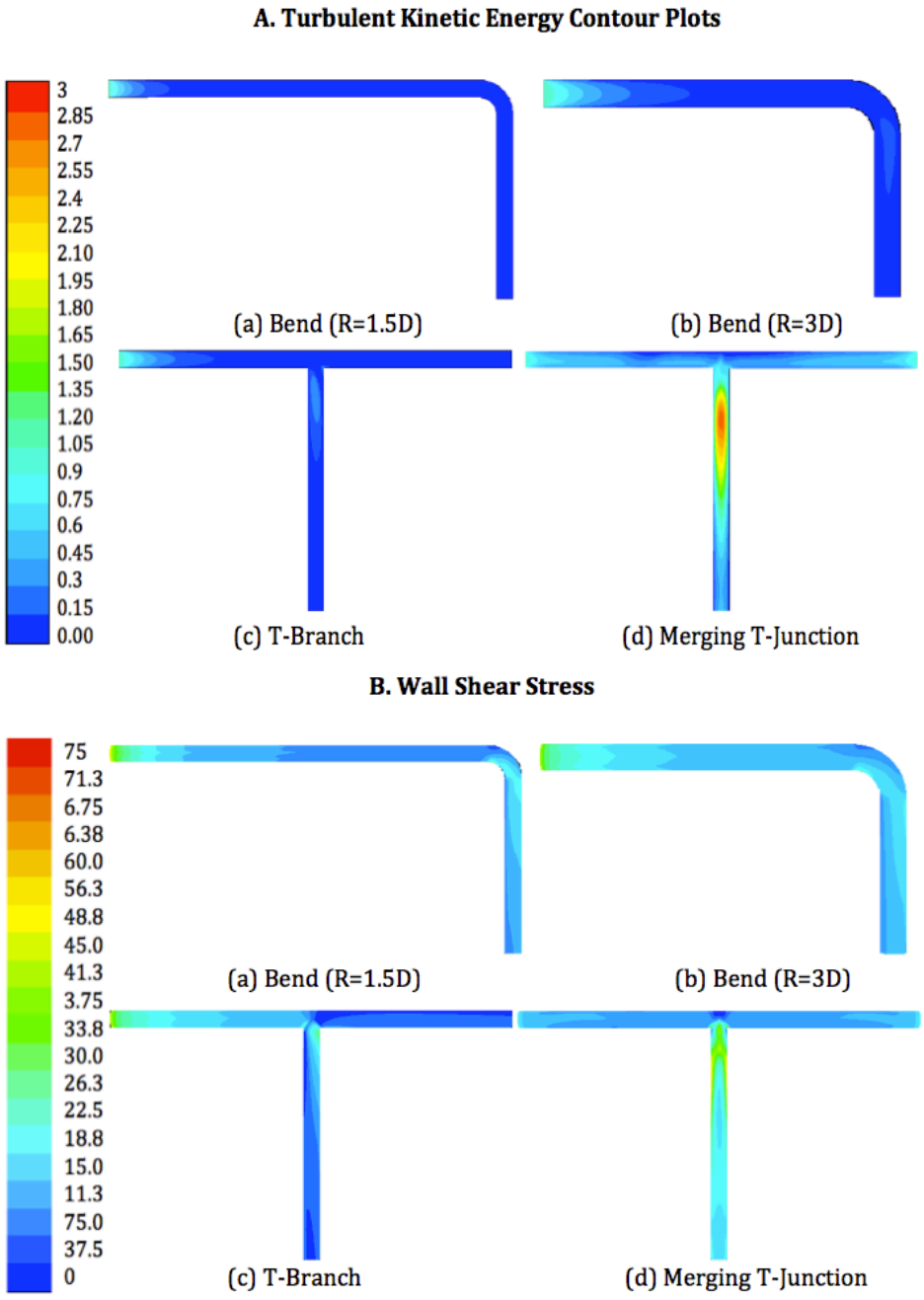

Figure 22: Contour Plots of (A) Turbulent Kinetic Energy (B) Wall Shear Stress at Flow Speed 2.5 m/s

From plots similar to what is shown in Figure 22, the value of the turbulent kinetic energy and wall shear stress at the point where the erosion/corrosion damage was most severe (according to the plant measurements), was recorded and used in the x-axes of the following plots, and the erosion/corrosion values were used on the y-axes. First, the erosion/corrosion values were plotted as a function of the turbulent kinetic energy for all of the 24 simulations that were run, as shown in Figure 23.

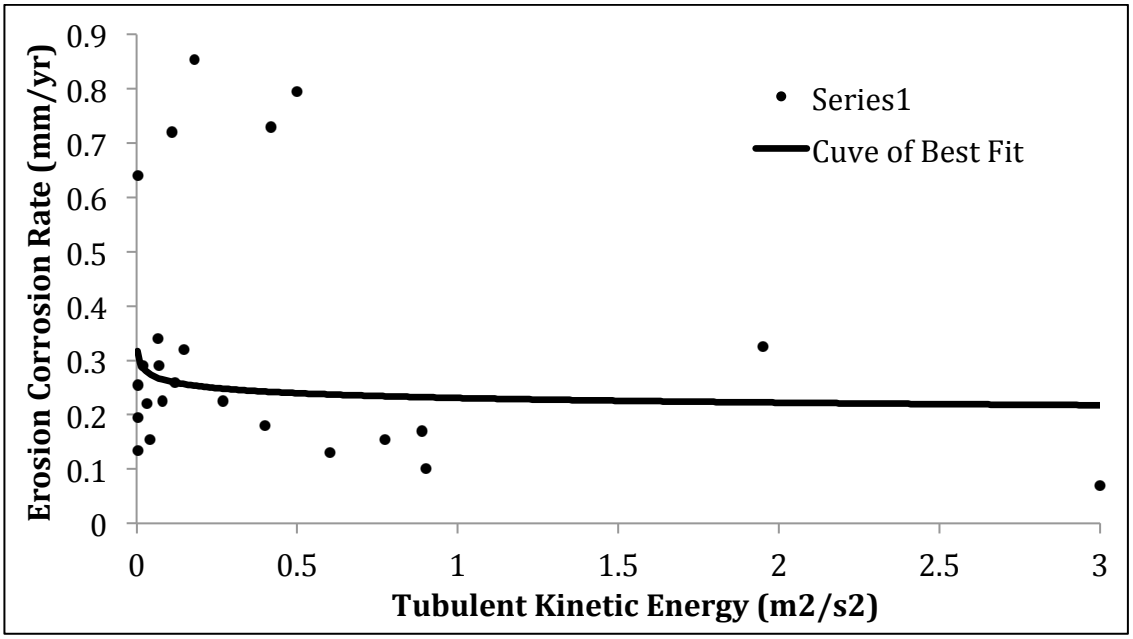

Figure 23: Erosion/Corrosion Plant Measurements as a Function of Turbulent Kinetic Energy

As shown in Figure 23, the relationship between erosion/corrosion and the turbulent kinetic energy has a decreasing trend, which agrees with what has been published in the literature. However, it was interesting to see whether the graph looks different if the data for each shape is plotted separately. Therefore, the graph of erosion/corrosion was plotted as a function of the turbulent kinetic energy (shown in Figure 24) for each shape separately, and again as a function of the wall shear stress (shown in Figure 25). The curve of best fit was also plotted for the set of data for each shape on the two graphs.

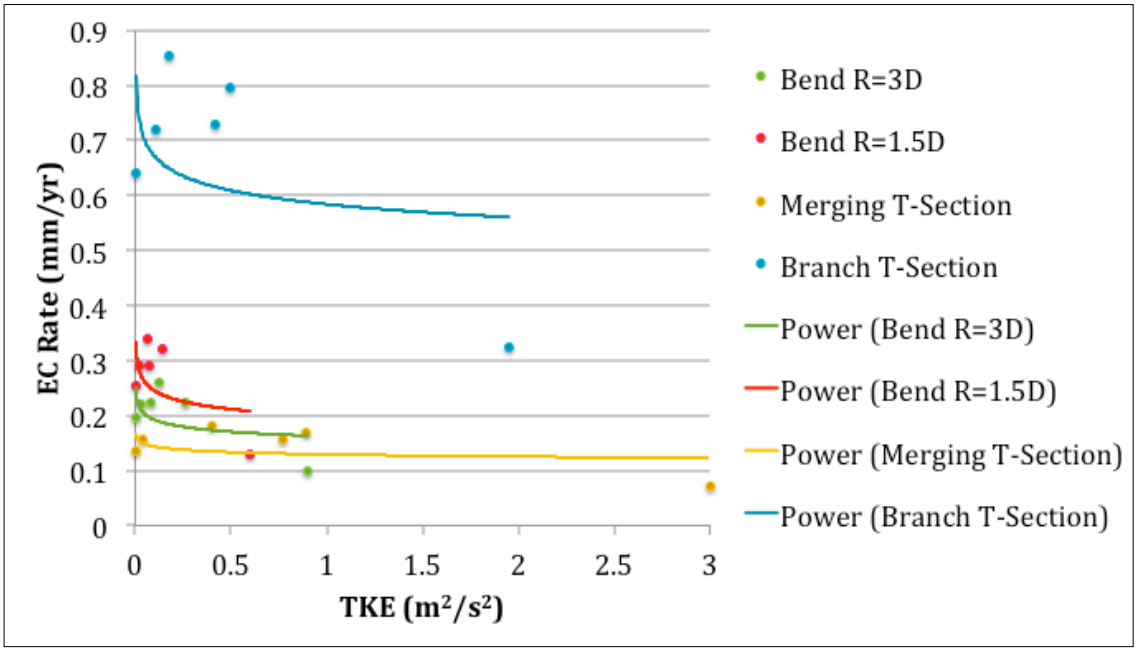

Figure 24: Erosion/Corrosion Plant Measurements as a Function of Turbulent Kinetic Energy for Each Shape

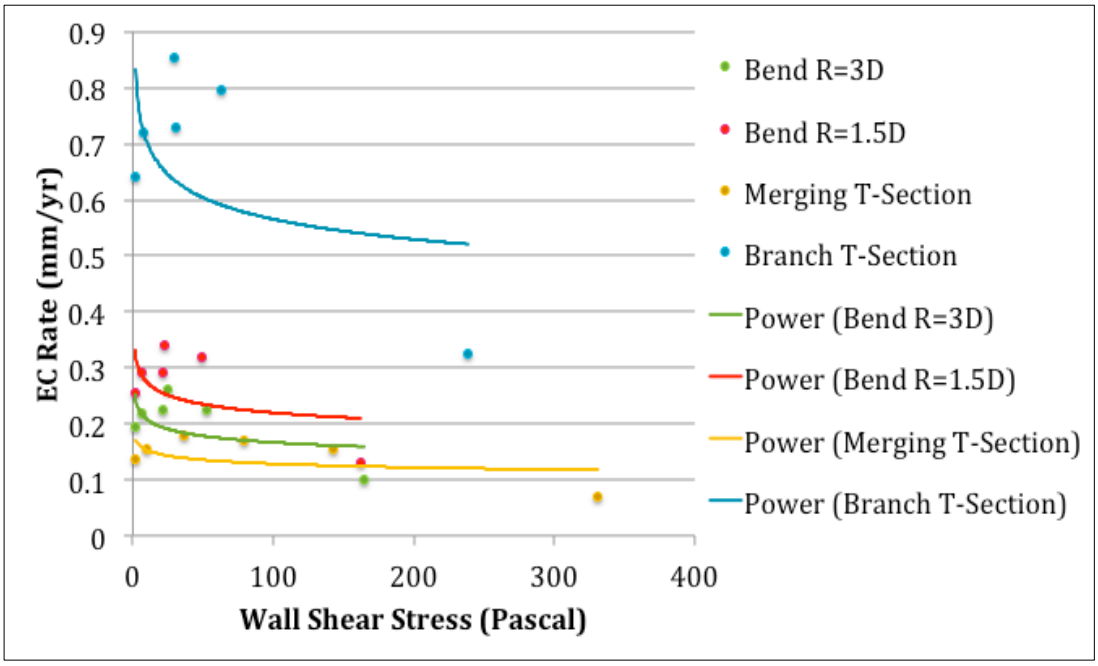

Figure 25: Erosion/Corrosion Plant Measurements as a Function of Wall Shear Stress for Each Shape

In both Figure 24 and Figure 25, the curve represents a best fit of the data points, using the noted function. The curve that seemed to fit the points best was a power function. As shown in both plots, looking at each shape separately, it is obvious that the decreasing trend that has been discussed before is still observed, which means that the same trend as what is published in the literature is obtained for each shape (Ferng and Lin, 2010).

By looking at the data of each shape separately, it was evident that the erosion/corrosion data had much higher values in the case of the T-branch than the rest of the geometries, even though the turbulent kinetic energy values, as predicted by FLUENT®, were generally within the same range for all pipes. In addition, the merging T-junction had the lowest erosion/corrosion values at similar turbulent kinetic energy values as the rest of the shapes. Moreover, the pipe bend with the sharper angle (R=1.5D) had higher erosion/corrosion values than the smoother pipe bend. The same trend was obtained when the erosion/corrosion values were plotted against the wall shear stress values. This shows that there must be another factor that causes the erosion/corrosion to be much more severe in the case of the T-branch. This factor must be significantly higher in the T-branch as compared to the merging T-junction, and must be higher in the sharper bend (R=1.5D) than in the smoother one (R=3D).

Therefore, several other factors that were predicted by FLUENT® were studied. Particularly, the dynamic pressure showed very interesting results. It was found that, in the case of the T-branch, as the flow enters the branch, it imposes high dynamic pressure at the point where the flow hits the wall. This is shown in Figure 26, which shows the dynamic pressure contour plot of an internal plane of the pipe.

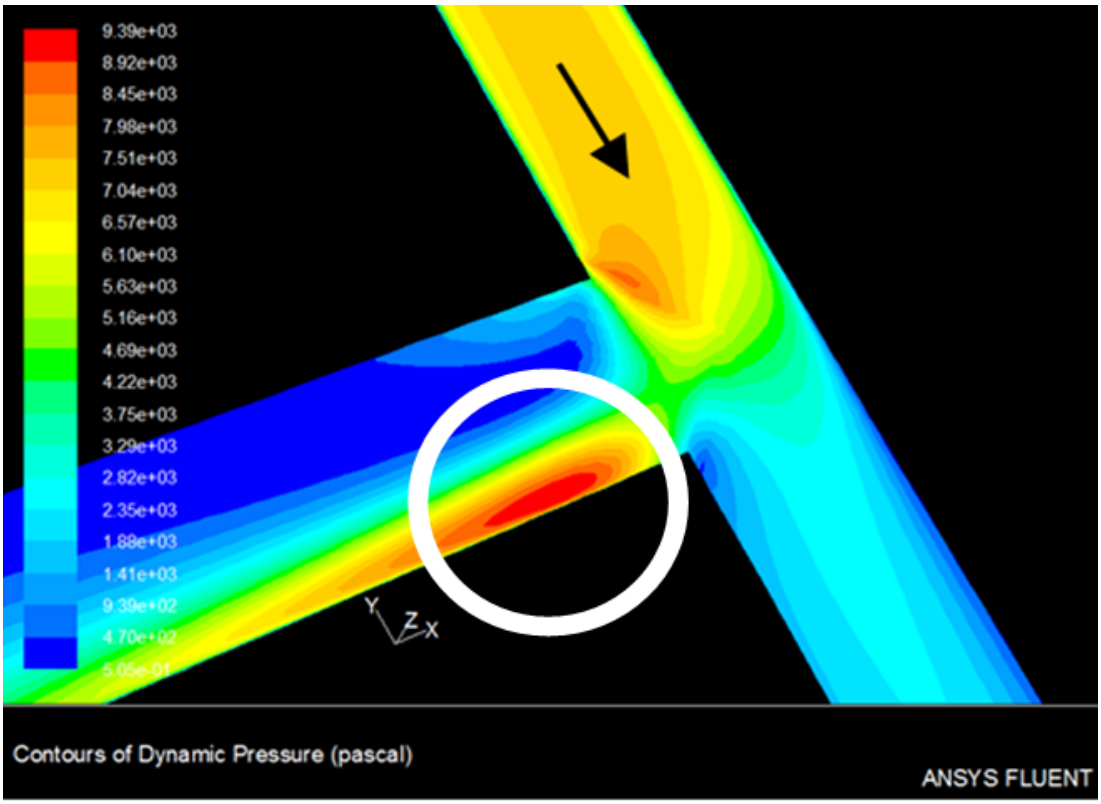

Figure 26: Dynamic Pressure Contour Plot of T-Branch

The arrow on Figure 26 represents the direction of the flow inside of the pipe, and the white circle points out the area where the dynamic pressure is highest. On the other hand, by looking at the same plot for the merging T-section, it is clear that the point of highest impact is actually where the flow from both inlets meets. In other words, the highest dynamic pressure is not imposed on the walls; it rather occurs before the flows hit the walls of the branch, as shown in Figure 27.

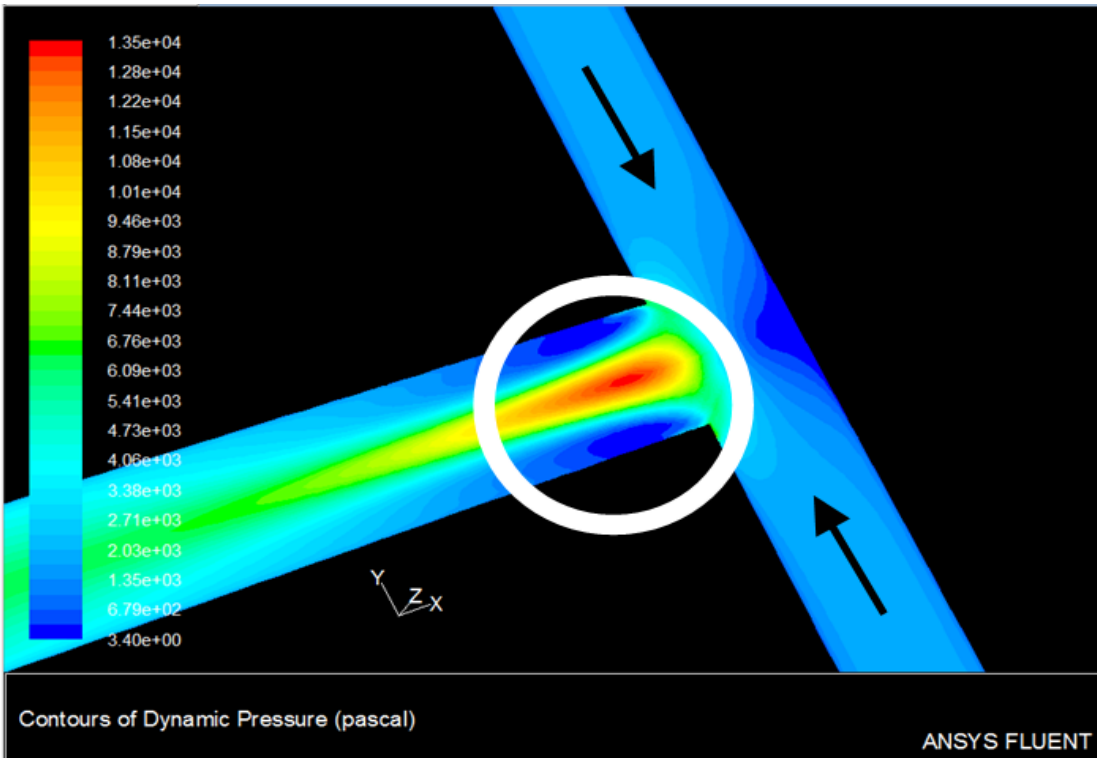

Figure 27: Dynamic Pressure Contour Plot of Merging T-Junction

Similarly, the maximum dynamic pressure was evidently higher in the case of the sharper pipe bend than in the bend with the larger radius. To quantify these results, the highest dynamic pressure for each shape at four speeds (1.2, 2.4, 2.5, and 3.6 m/s) was plotted, and is shown in Figure 28.

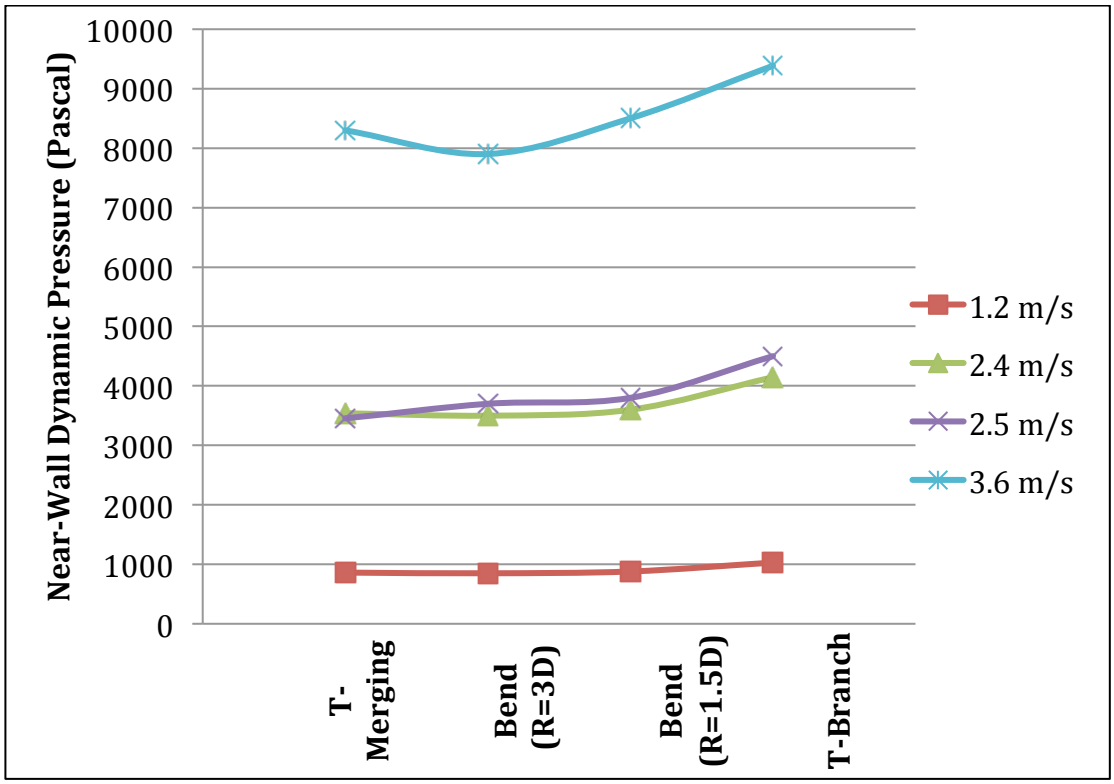

Figure 28: Near-Wall Dynamic Pressure at Different Velocities for Each Shape

In Figure 28, the dynamic pressure was plotted for 4 of the speeds. The other two speeds that the simulations were run at (0.26 and 7.5 m/s) had very extreme values, causing the trends shown by the other data points seem negligible, and therefore were not used in this study. The points shown in Figure 26 show that the dynamic pressure had a general increasing trend with velocity, and that the T-branch had significantly higher values than the rest of the shapes. The bend with the elbow radius to diameter ratio of 1.5 then had the second highest dynamic

pressure values, agreeing with the trend shown by the erosion/corrosion data. The other bend and the merging T-junction had very close dynamic pressure values.

It is important to note that the dynamic pressure is a function of the flow velocity squared and is given by the following function:

$$q = \frac{1}{2}\rho v^2$$

where: q is the dynamic pressure

ρ is the density of the flow

v is the velocity of the flow

Since the main purpose of this study was to investigate the effect of the change in geometry on the erosion/corrosion values, and not the change in velocity, it was necessary to normalize the dynamic pressure values. Therefore, the dynamic pressure values were normalized with respect to the merging T-junction values, in order to account for the velocities that are squared in the dynamic pressure equation. After that, the normalized dynamic pressure values were plotted for each shape at each of the four velocities. This plot is shown in Figure 29.

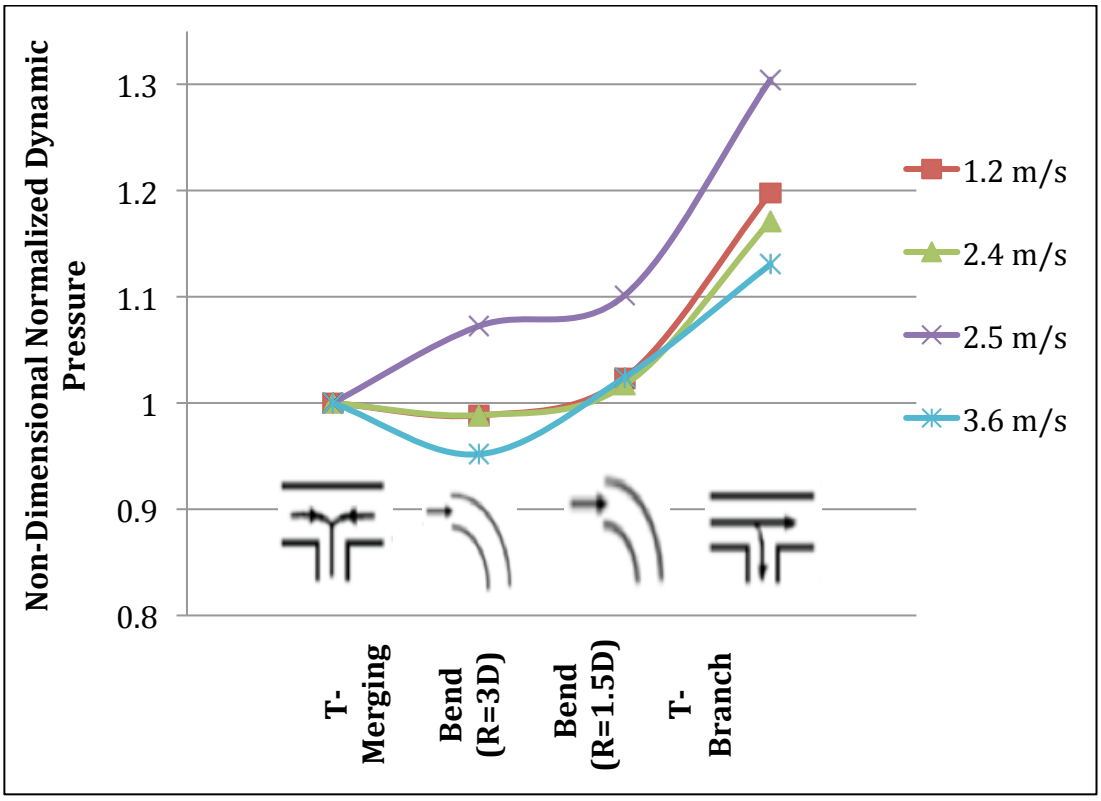

Figure 29: Maximum Dynamic Pressure for Each Shape at Four Different Speeds

As clear from Figure 29, the dynamic pressure is much higher in the T-branch than the rest of the other geometries, the sharper elbow has higher dynamic pressure than the smoother one, and finally, the merging T-junction has the same or lower dynamic pressure values than the smoother bend. This trend is consistent with the trend that the erosion/corrosion data showed. Therefore, the erosion/corrosion

values were plotted against the dynamic pressure values. This plot is shown in Figure 30.

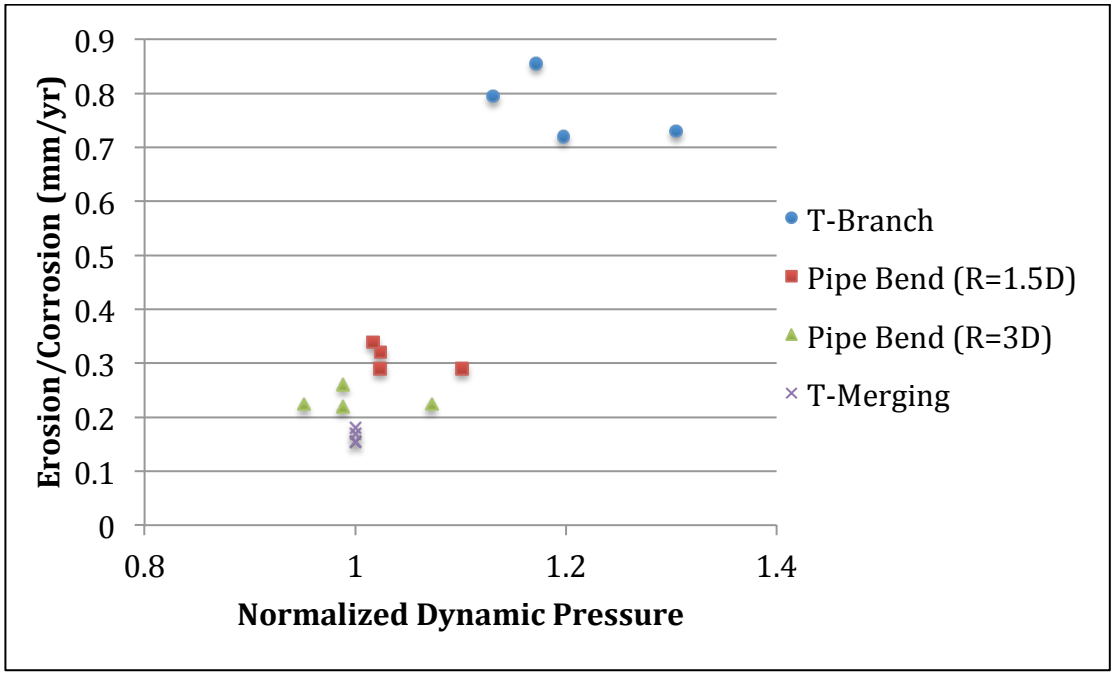

Figure 30: Erosion/Corrosion as a Function of Normalized Dynamic Pressure

While the data points on Figure 30 are somewhat scattered, there is a general increasing trend that shows that as the dynamic pressure increases, the erosion/corrosion increases as well. This shows that while the turbulence and wall shear stress do have an effect on the erosion/corrosion values, the dynamic pressure on the walls of the pipes also has a great effect on the erosion/corrosion rates.

5.7 Conclusion

The main conclusions that can be drawn from this analysis are the following:

- The flow turbulence and the shear stress imposed by the flow on the surface of the pipe from CFD predictions have highest values where erosion/corrosion had occurred.
- The erosion/corrosion values from the literature were highest for the T-branch and lowest for the merging T-junction, with the two bends with values in between. However, the turbulence and wall shear stress values, predicted by CFD were within the same range.
- The dynamic pressure follows the same trend as the erosion/corrosion: it is highest for the T-branch, lowest for the merging T-junction, and higher in the R=1.5D bend than the R=3D bend, both of which have values between the T-branch and merging T-junction.
- The dynamic pressure has a significant effect on the erosion/corrosion rate.
- Flow turbulence and wall shear stress may be used to indicate where erosion/corrosion will take place in the future.
- Dynamic pressure may be used to indicate how much erosion/corrosion would take place.

In order to understand this relationship better, more data is required to better quantify this trend and possibly develop empirical formulae for each shape to

relate the wall thinning rate due to erosion/corrosion to flow hydrodynamic factors such as the flow turbulence, wall shear stress and dynamic pressure.

6. CONCLUSIONS

6.1 Summary

In this work, a thorough study of corrosion, a problem most industries have been struggling with for decades, was carried out. An overview of the most common types of corrosion was given, which included: generalized corrosion, pitting, galvanic cell, crevice, concentration-cell, microbially induced corrosion, as well as corrosion under insulation and erosion/corrosion, both of which this thesis focused on. Moreover, the inspection methods that are most commonly used nowadays have been outlined. The methods that were discussed include: visual inspection, ultrasonic and acoustic testing, radiographic methods and electromagnetic methods.

After that, corrosion under insulation was studied more extensively and a different potential method of inspection of it was investigated, namely, X-ray computed tomography. The reason a new method of inspection for corrosion under insulation was studied, is that even though the CUI problem has been discovered for years, it is still causing many severe incidents and costing the industry plenty in terms of money and downtime. Finally, an intensive analysis on erosion/corrosion was conducted through CFD modeling. Erosion/corrosion is also a major problem in the industry, although it tends to be prevalent in some processes more than others.

Here the relationship between the behavior of the flow inside pipes of different shapes was studied and correlated to the erosion/corrosion rates.

6.2 Conclusions

From the X-ray tomography analysis, it was concluded that this method has a lot of potential in detecting both external and internal corrosion simultaneously, accurately, without requiring the insulation layer to be removed. The output of this method is a 3D image of the pipe being tested that can be visualized from all directions on the computer screen. Moreover, it was found that the type of insulation jacketed around the pipe does not affect the accuracy of the results, since the density of the insulation is insignificant compared to that of the metal.

As for the erosion/corrosion CFD studies, it was found that as the turbulence of the flow and the shear stress that is imposed by the flow on the surface of the pipe increase, the erosion/corrosion rate decreases. Although at low values, they both increase the rate of erosion/corrosion. This trend is consistent with what has been published in the literature about the relationship between erosion/corrosion and the flow turbulence. However, it was found that one of the reasons why different pipe shapes have different erosion/corrosion rates is the dynamic pressure that is imposed by the flow on the surface.

6.3 Future Work

The X-ray tomography system that was used for the experiments described earlier is a large system that would not be very practical to use on sites to carry out corrosion inspections regularly. Therefore, suggested future work would be to investigate in a portable X-ray tomography system and study the safety implications of it, which might include radiation.

Moreover, more plant data should be gathered and used to carry out more CFD simulations in the erosion/corrosion section, and generalize the trends observed in the preliminary runs that were done in this work. This data should be used to:

- Predict turbulence, wall shear stress, and dynamic pressure inside more different geometries
- Develop empirical formulae to help predict EC in different pipes based on the hydrodynamic factors of different flows

REFERENCES

Agarwala, V., Reed, P., & Ahmad, S. (2000). *Corrosion Detection and Monitoring - A Review.* Orlando, Fl: NACE International.

Al-Darbi, M., Muntasser, Z., Tango, M., & Islam, M. (2002). Control of Microbial Corrosion Using Coatings and Natural Additives. *Energy Sources*, *24*(11), 1009-1018.

Balasko, M., Svab, E., Kuba, A., Kiss, Z., Rodek, L., & Nagy, A. (2005). Nuclear Instruments and Methods in Physics Research Section A: Accelerators Spectrometers, Detectors and Associated Equipment. *Fifth International Topical Meeting on Neutron Radiography*, 302-308. Budapest, Hungary: Fifth International Topical Meeting on Neutron Radiography.

Barker, R., Hu, X., Neville, A., & Cushnaghan, S. (2011). Flow-Induced Corrosion and Erosion-Corrosion Assessment of Carbon Steel Pipework in Oil and Gas Production. *NACE International.* Houston, Tx: NACE International.

Beavers, J., & Thompson, N. (2006). External Corrosion of Oil and Natural Gas Pipelines. *ASM Handbook, 13C*, 1015-1025. Materials Park, Oh: ASM International.

Beck, M., Goebbels, J., Burkert, A., Isecke, B., & Babler, R. (2010). Monitoring of Corrosion Processes in Chloride Contaminated Mortar by Electrochemical Measurements and X-Ray Tomography. *Materials and Corrosion*, *61*(6), 475-479.

Bush, S. (1990). The Effects of Erosion-Corrosion on Power Plant Piping. *59th General Meeting of the National Board of Boiler and Pressure Vessel Inspector.* National Board BULLETIN. Available online 10 January 2012. http://www.nationalboard.org/index.aspx?pageID=164&ID=213

Callister, W. (1972). Profile Radiography by Gamma Rays. *Non-Destructive Testing*, *5*(4), 214-219.

Carreon, L., Glassman, S., Schwender, J., Subach, B., & Gornet, M. (2008). Reliability and Accuracy of Fine-Cut Computed Tomography Scans to Determine the Status of Anterior Interbody Fusions with Metallic Cages. *The Spine Journal*, *8*(6), 998-1002.

CC Technologies. (2008). *Metallurgical Analysis of 24-Inch Houstonia 200 Service Failure at MP 21.6 (8/25/08).* Dublin, Ireland: CC Technologies, Inc.

Chawla, S., & Gupta, R. (1993). *Materials Selection for Corrosion Control.* Materials Park, Oh: ASM International.

ClassNK. (2008). *Guidelines on Pipeline Wall Thinning -Taking into Account Flow Accelerated Corrosion of Water and Wet Steam Pipelines in Ships.* Chiyoda-ku, Japan: ClassNK.

Corrosion Between Anodized Aluminum and Steel. (2009). Available online 23rd February 2012. http://aluminumsurface.blogspot.com/2009/04/corrosion-between-anodized-aluminum-and.html

Department of Transportation Pipeline and Hazardous Materials Safety Administration . (2008). *Williams Transcontinental Gas Pipe Line Corp. -CPF No. 1-2008-1004H.* Washington, D.C.: Department of Transportation Pipeline and Hazardous Materials Safety Administration .

Department of Transportation Pipeline and Hazardous Materials Safety Administration Office of Pipeline Safety. (2006). *Tennessee Gas Pipeline, An Affiliate of El Paso Corporation -CPF No.2-2006-1007H.* Washington, D.C.: Department of Transportation Pipeline and Hazardous Materials Safety Administration Office of Pipeline Safety.

Fagaly, R. (2006). Superconducting Quantum Interference Device Instruments and Applications. *Rev Sci Instrum*, *77*(10), 101-146.

Ferng, Y., & Lin, B. (2010). Predicting the wall thinning engendered by erosion–corrosion using CFD methodology. *Nuclear Engineering and Design, 240*(10), 2863-2841. Washington, D.C.: Elsevier.

Galvanic Compatability Corrosion Dissimilar Metal Corrosion. Available online 19th January 2012. http://www.engineersedge.com/galvanic_capatability.htm

Hansen, D., Davenport, A., Lillard, R., Fujimoto, S., & Buchheit, R. (2009). Corrosion (General) -215th ECS Meeting. *ECS Meeting, 19*(29), 167-168. Pennington, NJ: The Electrochemical Society.

Health and Safety Executive. (2001). *Public Report of the Fire and Explosion at the ConocoPhillips Humber Refinery*. Sudbury, UK: HSE.

Howard, B., Gibbs, K., & Elder, J. (2003). *Corrosion Detection Devices.* Aiken, South Carolina: U.S. Department of Energy.

Industrial Nanotech, Inc. (2006). *Corrosion Under Insulation (CUI) A Nanotechnology Solution.* Naples, Fl: Industrial Nanotech, Inc.

Keeping Pipelines Safe from Internal Corrosion. (2011). Available online 25th February 2012. http://www.ien.com/article/keeping-pipelines-safe/4252

Koch, G., & Thompson, N. (2002). *Corrosion Costs and Preventive Strategies in the United States.* McLean: U.S. Federal Highway Administration.

Little, D., Massad, E., & Kassem, E. (2009). *Advanced Characterization of Infrastructure Materials Laboratory.* College Station: Zachry Department of Civil Engineering.

National Wildlife Federation. (2010). *Full Oil Incident List by State.* Available online 12th December 2011. http://www.nwf.org/News-and-Magazines/Media-Center/News-by-Topic/Global-Warming/2010/~/media/PDFs/Global%20Warming/Reports/Full-Oil-Incident-List.ashx

Piper, J. (1999). *Operations and Maintenance Manual for Energy Management.* Armonk, NY: M. E. Sharpe, Inc.

Rashidi, N., Alavi-Soltani, S., & Asmatulu, R. (2007). Crevice Corrosion Theory, Mechanisms and Prevention Methods. *3rd Annual GRASP Symposium,* 215-216. Wichita, Ks: Annual GRASP Symposium.

Redmer, B., Ewert, U., & Neundorf, B. (2007). Developments in Radiographic Inspection Methods: TomoCAR -Tomographical Computer-Aided Radiography - a New Testing Method for the Visualisation and Sizing of Defects in Circumferential Seams. *6th International Conference on NDE in Relation to Structural Integrity for Nuclear and Pressurized Components.* Budapest, Hungary: International Conference on NDE.

Sidener, C. (2009). *Company Fined in Appomattox Pipeline Explosion.* Available online 21st February 2012. http://www2.newsadvance.com/news/2009/aug/10/company_fined_in_appomattox_pipeline_explosion-ar-214395/

Tada, T., Suetsugu, H., & Mori, H. (2010). *Inspection Technique for CUI (Corrosion under Insulation) by Using Fiber Optical AE Sensor.* Chuo-ku: Sumitomo Chemical Co, Ltd.

Torczynski, J., O'Hern, T., Adkins, D., Jackson, N., & Shollenberger, K. (1997). *Advanced Tomographic Flow Diagnostics for Opaque Multiphase Fluids.* Springfield, VA: National Technical Information Service.

Twomey, M. (1997). *Back to Basics -Inspection Techniques for Detecting Corrosion Under Insulation.* Available online 28th September 2011. http://www.asnt.org/publications/materialseval/basics/feb97basics/feb97basics.htm

Ultrasonic Nondestructive Testing -Advanced Concepts and Applications. (2012). Available online 27th March 2012. http://zone.ni.com/devzone/cda/tut/p/id/5369

United States Nuclear Regulatory Commission Office of Nuclear Reactor Regulation. (2006). *NRC Information Notice 2006-08: Secondary Rupture at the Mihama Power Station in Japan.* Washington, D.C.: NRC.

US Department of Defense. (2003). *Unified Facilities Criteria (UFC) -Operation and Maintenanace: Cathodic Protection Systems.* Department of Defense.

Wanga, X., & Wong, B. (2005). Image Enhancement for Radiography Inspection. *3rd International Conference on Experimental Mechanics, 10*(4), 462-468. Singapore: SPIE.

Wassink, C. (2008). *Comparison of Guided Waves Inspection and Alternative Strategies for Inspection of Insulated Pipelines*. Saarbrucken, Germany. Available online 15 March 2012. http://www.ndt.net/article/dgzfp-utgw-2008/Paper04.pdf

Wendt, J. (2009). *Computational Fluid Dynamics An Introduction.* Berlin: Spinger-Verlag Berlin Heidelberg.

Wood, M. (2010). *Corrosion Accidents in Refineries -Preliminary findings from a study of recent accidents in OECD/EU countries.* Brussels, Belgium: JRC.

APPENDIX A

CORROSION UNDER INSULATION DETECTION

X-Ray Computed Tomography Apparatus

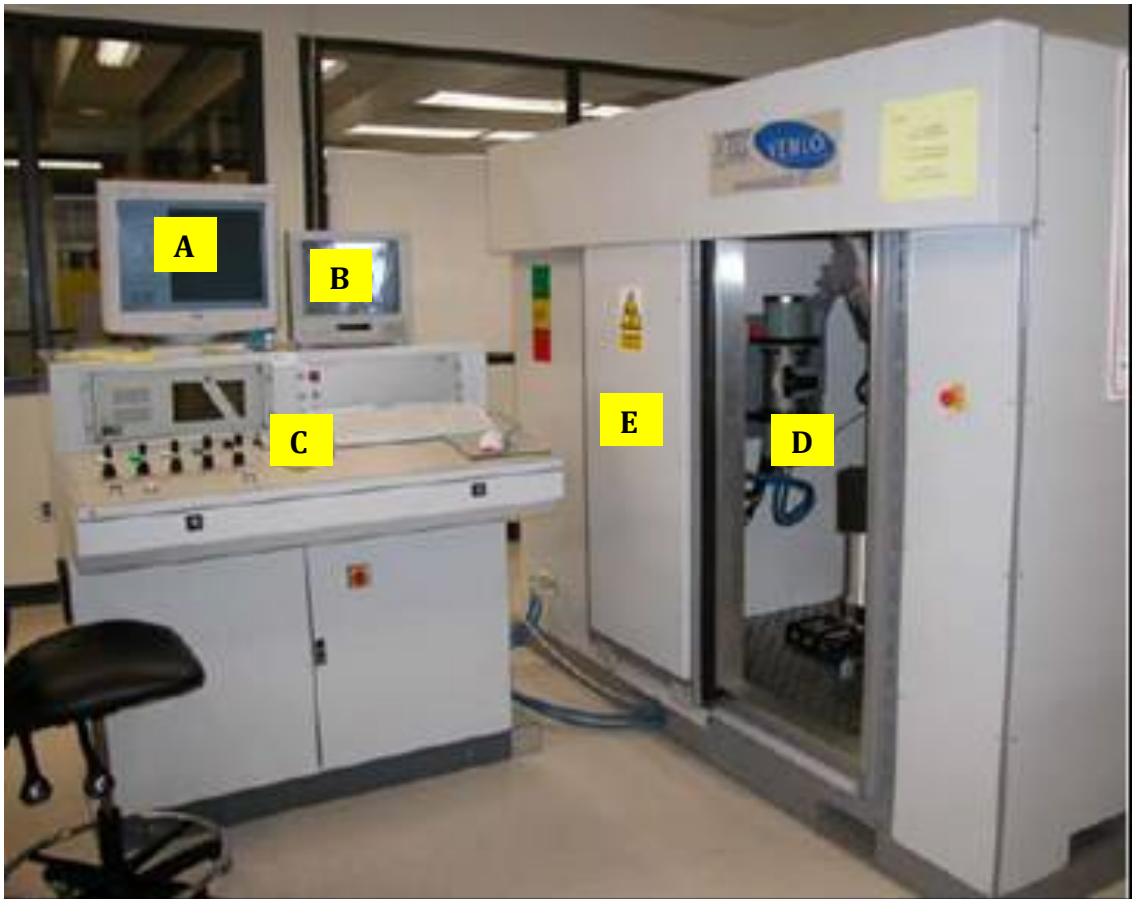

Figure A-1: X-Ray Computed Tomography System

A- Computer screen where results are displayed
B- Computer screen where specimen inside the X-ray chamber is monitored
C- System controllers
D- X-ray chamber (refer to Figure A-2 for more details)
E- X-ray chamber slide door

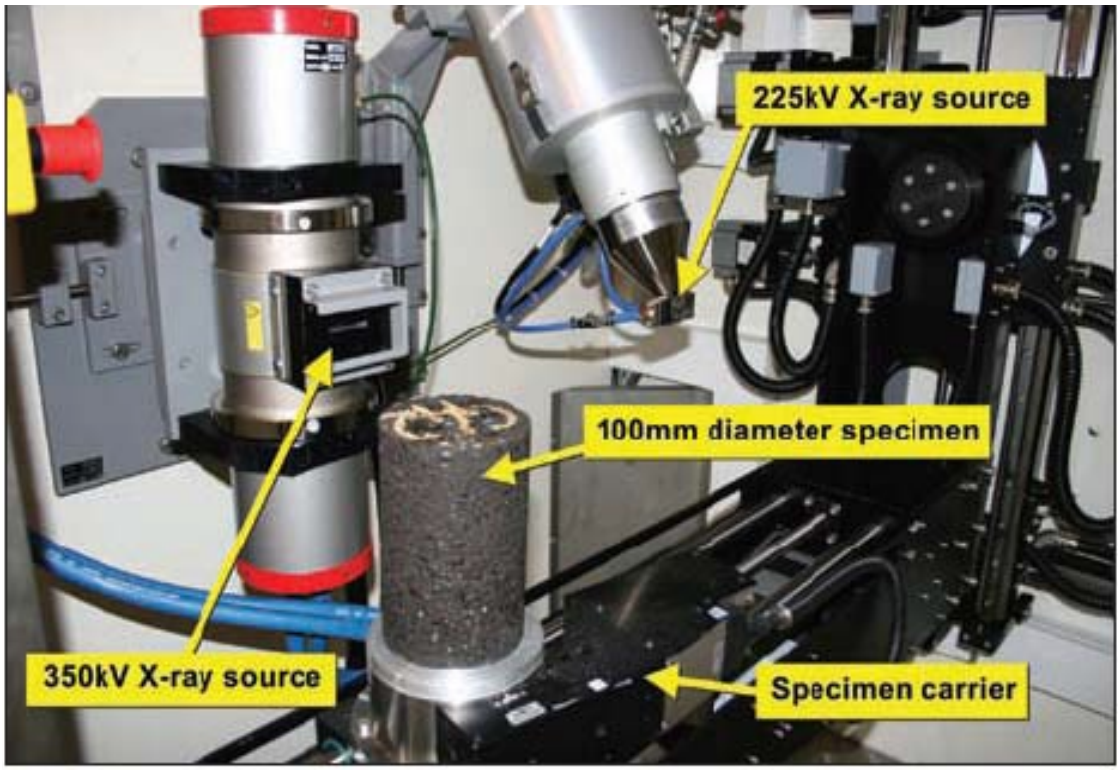

Figure A-2: Details of the interior of the X-ray Chamber

APPENDIX B

EROSION/CORROSION PREDICTION

Grid Independence Study

To ensure that the number of nodes used in the simulations was sufficient to make accurate predictions of the flow behavior, a grid independence study was carried out. The differential pressure predicted at the maximum speed used (7.5 m/s) was recorded for the number of nodes used for each pipe shape. Then the number of nodes was increased twice and the differential pressure was also recorded. The percentage difference in the differential pressure was plotted as a function of the number of nodes. The results are displayed in Table B-1 and also in Figure B-1.

Table B-1: Grid Independence Study

Pipe Bend (R=1.5D), 7.5 m/s			
	Used	Higher	Highest
Number of Nodes	700,000	7.40E+05	1.20E+06
Delta P (Pa)	17600.26	17585.5	17726.8
Percentage %	0	0.084	0.7189
Pipe Bend (R=3D), 7.5 m/s			
	Used	Higher	Highest
Number of Nodes	441,225	6.78E+05	7.20E+05
Delta P (Pa)	12636.2	12824.6	12854
Percentage %	0	1.491	1.723
T-Merging, 7.5 m/s			
	Used	Higher	Highest
Number of Nodes	562,836	6.25E+05	8.25E+05
Delta P (Pa)	55486.3	54916.6	55997.9
Percentage %	0	1.027	0.922
T-Branch, 7.5 m/s			
	Used	Higher	Highest
Number of Nodes	562,836	6.25E+05	7.20E+05
Delta P (Pa)	16507.72	16379.5	16488.2
Percentage %	0	0.777	0.1182

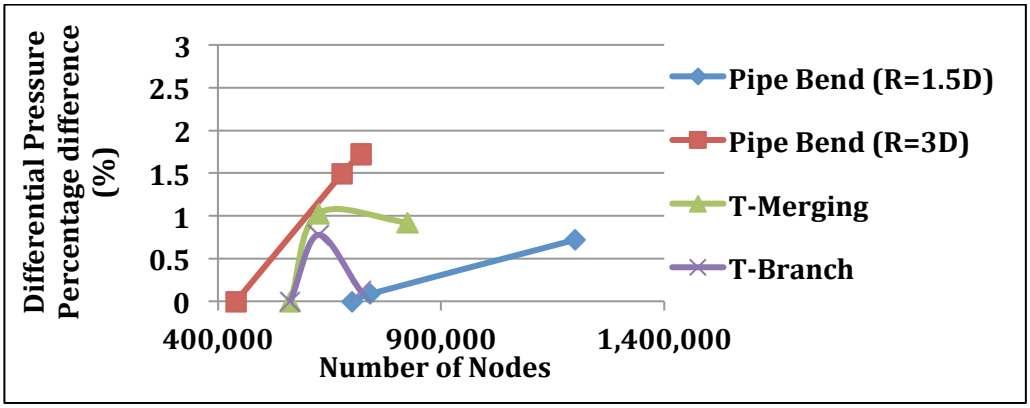

Figure B-1: Differential Pressure Percentage Difference as a Function of Number of Nodes

The results of this study show that any increase in the number of nodes has a very negligible effect on the results (less than 2%) in the worst case. Therefore, the number of nodes that was used in the simulations was sufficient to make accurate predictions of the flow.

Tables Used in Figures

Shape	Speed (m/s)	Maximum Turbulent Kinetic Energy (near-wall) (m^2/s^2)	Maximum Wall Shear Stress (Pascal)	Maximum EC Rate (mm/yr)
Pipe bend (R=3D)	**1.2**	0.032	6.67	0.22
	2.5	0.08	21	0.225
	3.6	0.267	52.5	0.225
	2.4	0.121	24.6	0.26
	0.26	0.003	1.34	0.195
	7.5	0.9	165	0.1
Pipe bend (R=1.5D)	**1.2**	0.018	6.03	0.29
	2.5	0.071	21.5	0.29
	3.6	0.146	48.7	0.32
	2.4	0.066	22.3	0.34
	0.26	0.00335	1.4	0.255
	7.5	0.6	162	0.13
T-section (merging)	**1.2**	0.04	10.011	0.155
	2.5	0.772	142.5	0.155
	3.6	0.89	78.8	0.17
	2.4	0.4	36.64	0.18
	0.26	0.005	2.26	0.135
	7.5	3	331	0.07
T-section (branch)	**1.2**	0.11	7.84	0.72
	2.5	0.42	31	0.73
	3.6	0.5	62.7	0.795
	2.4	0.18	29	0.855
	0.26	0.0041	1.68	0.64
	7.5	1.95	238.5	0.325

Shape	Speed (m/s)	Maximum EC Rate (mm/yr)	Dynamic Pressure	Standardized Dynamic Pressure
Pipe bend (R=3D)	**1.2**	0.22	850	0.988372093
	2.5	0.225	3700	1.072463768
	3.6	0.225	7900	0.951807229
	2.4	0.26	3500	0.988700565
	0.26	0.195	52	11.30434783
	7.5	0.1	34500	0.913907285
Pipe bend (R=1.5D)	**1.2**	0.29	880	1.023255814
	2.5	0.29	3800	1.101449275
	3.6	0.32	8500	1.024096386
	2.4	0.34	3600	1.016949153
	0.26	0.255	45	9.782608696
	7.5	0.13	25600	0.678145695
T-section (merging)	**1.2**	0.155	860	1
	2.5	0.155	3450	1
	3.6	0.17	8300	1
	2.4	0.18	3540	1
	0.26	0.135	4.6	1
	7.5	0.07	37750	1
T-section (branch)	**1.2**	0.72	1030	1.197674419
	2.5	0.73	4501	1.304637681
	3.6	0.795	9385	1.130722892
	2.4	0.855	4147	1.171468927
	0.26	0.64	55.5	12.06521739
	7.5	0.325	41461	1.098304636

VITA

Sally Samir Farid Nicola received her Bachelor of Science degree in chemical engineering from Texas A&M University at Qatar in May 2010. She enrolled in the Master of Science in safety engineering program at Texas A&M University, College Station, Texas in September 2010 and joined the Mary Kay O'Connor Process Safety Center at the same time. She received her M.S. in safety engineering in August 2012.

Ms. Nicola may be reached at Jack E. Brown Engineering Building, 3122 TAMU Room 200, College Station, Texas-77843, or via email at sally.nicola@gmail.com.